

Minimal surfaces in the roto-translation group with applications to a neuro-biological image completion model

Robert K. Hladky

*Department of Mathematics, Dartmouth College, 6188 Bradley Hall
Hanover, NH 03755 USA*

robert.k.hladky@dartmouth.edu

Scott D. Pauls

*Department of Mathematics, Dartmouth College, 6188 Bradley Hall
Hanover, NH 03755 USA*

scott.d.pauls@dartmouth.edu

We investigate solutions to the minimal surface problem with Dirichlet boundary conditions in the roto-translation group equipped with a subRiemannian metric. By work of G. Citti and A. Sarti, such solutions are amodal completions of occluded visual data when using a model of the first layer of the visual cortex. Using a characterization of smooth minimal surfaces as ruled surfaces, we give a method to compute a minimal spanning surface given fixed boundary data presuming such a surface exists. Moreover, we describe a number of obstructions to existence and uniqueness but also show that under suitable conditions, smooth minimal spanning surfaces with good properties exist. Not only does this provide an explicit realization of the disocclusion process for the neurobiological model, but it also has application to constructing disocclusion algorithms in digital image processing.

Keywords: Minimal surfaces, Carnot-Carathéodory spaces, vision, occlusion

AMS Subject Classification: 53C17, 49Q05, 92B05

1. Introduction

The study of minimal and isoperimetric surfaces in Carnot-Carathéodory spaces has recently received a good deal of attention.^{2, 3, 6–9, 12, 17, 18, 20, 21, 24} In the work cited, the various authors explore the existence, uniqueness and properties of minimal and isoperimetric problems, finding that, at least in specific lower dimensional cases, the minimal/isoperimetric surfaces have a rich geometric structure. Moreover, recent work of Citti, Manfredini and Sarti^{4, 5} has provided a link between the method by which the brain completes missing visual data in the first layer of the visual cortex (V1) and the solutions to the minimal surface problem in a specific Carnot-Carathéodory space, the roto-translation group, that arises in a mathematical model of the function of V1. In this paper, we denote the roto-translation group by \mathcal{RT} . It is homeomorphic to $\mathbb{R}^2 \times \mathbb{S}^1$ and we will use (x, y, θ) as coordinates. Following the construction of Citti and Sarti, we define a Carnot-Carathéodory structure on

2 Robert K. Hladky and Scott D. Pauls

\mathcal{RT} by distinguishing a horizontal subbundle, \mathcal{H} , given by the span of the following two vector fields at each point:

$$X_1 = \cos(\theta) \frac{\partial}{\partial x} + \sin(\theta) \frac{\partial}{\partial y}, \quad X_2 = \frac{\partial}{\partial \theta}.$$

These two vector fields bracket generate the tangent bundle and form a distribution of contact planes in this three dimensional space. Placing an inner product on \mathcal{H} which makes $\{X_1, X_2\}$ an orthonormal basis for \mathcal{H} , we have the standard Carnot-Carathéodory distance on \mathcal{RT} :

$$d_{cc}(a, b) = \inf_{\gamma \in \mathcal{A}} \left\{ \int \langle \gamma', \gamma' \rangle^{\frac{1}{2}} \left| \gamma(0) = a, \gamma(1) = b \right| \right\}$$

where \mathcal{A} is the set of absolutely continuous paths whose derivatives, when they exist, are in \mathcal{H} .

In this model, a greyscale image, $I : \Omega \subset \mathbb{R}^2 \rightarrow \mathbb{R}$, has a representation in \mathcal{RT} given by

$$\Sigma = \left\{ (x, y, \theta) \left| \theta = \arctan \left(-\frac{I_x}{I_y} \right) \right. \right\}.$$

If a portion of the image is occluded in a domain $\Omega_0 \subset \Omega$, then Citti and Sarti's model provides a completion of the occluded region by constructing a minimal spanning surface. More precisely, if $c \subset \Sigma$ is the curve in \mathcal{RT} associated to $\partial\Omega_0$, then the completion is given finding the minimal surface in \mathcal{RT} that spans c , i.e. a minimizer of the perimeter measure. For a C^1 surface, Σ , given as a level set of a C^1 function u , the perimeter is given by

$$\mathcal{P}(\Sigma) = \int \sqrt{(X_1 u)^2 + (X_2 u)^2} dA \quad (1.1)$$

Moreover we know that such minimal surfaces satisfy the following partial differential equation:

$$X_1 \left(\frac{X_1 u}{\sqrt{(X_1 u)^2 + (X_2 u)^2}} \right) + X_2 \left(\frac{X_2 u}{\sqrt{(X_1 u)^2 + (X_2 u)^2}} \right) = 0.$$

In addition to this relationship between the minimal surface problem and a model for biological image reconstruction, Citti and Sarti provide a reinterpretation of a number of existing algorithms for digital inpainting and image completion. In particular, Citti and Sarti⁵, and Citti, Manfredini and Sarti⁴, examine the variational models of Ambrosio-Masnou¹, and a variant of the Mumford-Shah functional and find that, under suitable interpretation in the roto-translation group model, minimizing these different functionals is equivalent to minimizing the standard Carnot-Carathéodory surface area functional given in equation (1.1). In other words, finding minimizers of these various functionals is equivalent to solving the Carnot-Carathéodory minimal surface problem in the roto-translation group.

In light of this unifying theme in the area of vision and image reconstruction, we explore the minimal surface problem in a class of groups which include the roto-translation group, \mathcal{RT} . Citti and Sarti show the divergence form of the minimal surface equation in \mathcal{RT} and we note that the more general framework of Cheng, Huang, Malchiodi and Yang³ shows both the divergence form equation and that the smooth minimal surfaces are ruled surfaces. We note that the characterization of minimal surfaces as ruled surfaces has generalizations in Carnot groups with two dimensional horizontal bundles¹² and Martinet-type spaces⁶.

In Section 4, we use the basic form of the minimal surface equation to explicitly derive the curves the rule smooth minimal surfaces in the roto-translation group. Specifically, we show that with respect to the Webster-Tanaka connection, ∇ , associated to a canonical pseudo-hermitian structure on \mathcal{RT} , the surfaces are foliated by ∇ -geodesics which, for fixed x_0, y_0, θ_0, R and $\dot{\theta} \neq 0$ take the form:

$$\begin{aligned} x(t) &= x_0 + R \sin(\theta(t)) \\ y(t) &= y_0 + R \cos(\theta(t)) \\ \theta(t) &= \theta_0 + \dot{\theta} t. \end{aligned}$$

Thus, we provide a geometric characterization of smooth minimal surfaces in the roto-translation group which in turn yields an explicit parametrization for every such minimal surface. In contrast to the existing methods of constructing minimal surfaces, which approximate a minimal surface via a diffusion mechanism, we note that this parameterization provides a method for constructing exact solutions to the minimal surface problem.

Second, we turn to understanding the occlusion problem in \mathcal{RT} . As demonstrated in the experimental evidence⁵, in the model of V1 given by the roto-translation group, representations of image data in \mathcal{RT} potentially contain different layers of conflicting data due to both modal and amodal completion of the image. In light of this finding, we focus on solving the occlusion problem by finding all possible smooth solutions or partial solutions of the minimal surface problem with a fixed boundary. In Section 6, we develop a test for determining when two points on a given curve can be joined by a ∇ -geodesic. We begin with a fixed curve, $c \subset \mathcal{RT}$, which is the boundary of an occluded region of the representation of an image in \mathcal{RT} and is parametrized as $c(t) = (\beta(t), \theta(t))$. For each point, $c(t_0)$ on c , we construct the set of other points on c accessible to $c(t_0)$, denoted $\mathcal{A}(c(t_0), c)$. To construct a portion of a smooth minimal surface we simply need construct a function:

$$u : D \subset \mathbb{S}^1 \rightarrow \mathbb{S}^1$$

where D is a connected subset of \mathbb{S}^1 and so that $u(t) \in \mathcal{A}(c(t), c)$. We note that to construct a smooth minimal spanning surface, we must have that $D = \mathbb{S}^1$. For each t , this function give a point $c(u(t))$ connected to $c(t)$ by a rule. Needless to say, there are numerous possibilities that occur when attempting to construct u . In particular, we note that we a guaranteed neither existence nor uniqueness of such

4 Robert K. Hladky and Scott D. Pauls

a u . A key tool in the analysis of $\mathcal{A}(c(t_0), c)$ is the transversality function given by

$$Q(t) = \theta(t) - \varphi_\beta(t)$$

where φ_β is defined by the equation

$$\frac{\beta'(t)}{|\beta'(t)|} = (-\sin(\varphi_\beta(t)), \cos(\varphi_\beta(t)))$$

To further examine this procedure, we simplify the investigation somewhat and restrict our consideration to curve c so that the projection of c to $\mathbb{R}^2 \subset \mathbb{R}^2 \times \mathbb{S}^1 = \mathcal{RT}$ is a circle. Under this assumption, we are able to describe a number of different cases ranging from cases where one can always find such a u , cases with multiple u and cases where no such u exists. In each of these cases, we give explicit examples using test image data and give some indication as to the cause of the various pathologies. The examples provide a number of obstruction to the existence and/or uniqueness of smooth minimal spanning surfaces.

On the positive side, after examining these various cases, we present a theorem showing sufficient conditions for when a smooth minimal completion exists.

Theorem 1.1. *Let $I : \mathbb{R}^2 \rightarrow \mathbb{R}$ be an intensity function of an image with an occlusion given by a circular region D . Further, suppose $\gamma \in \mathcal{RT}$ is the θ lift of ∂D and that the occlusion is completely nondegenerate and occludes no critical points of I . If $Q'(t) \neq 0$ for $t \in [0, 2\pi]$ then there exists a minimal spanning surface of γ where the projection of each rule of the surface lies in the interior of D . Moreover, if $Q'(t) < 0$ for $t \in [0, 2\pi]$ then the projection of this spanning surface to the xy -plane is surjective onto the occluded region.*

An occlusion is completely nondegenerate if there are no critical points of I on ∂D , only a finite number of critical points in the interior of D and an angle function can be extended continuously across those critical points (see below for a more precise definition).

We again emphasize that, in such a case, the construction of such a surface is significantly less computationally intensive than the iterative approximative method used by Citti and Sarti⁵. We expect that similar gains can be achieved with respect to the other models mentioned above such as the Ambrosio-Masnou and elastica methods. In this direction, we note that the authors¹¹ use a discrete version of the method used in this theorem to provide a new algorithm for disocclusion in the context of digital image reconstruction. Moreover, we expect that this method will have application to neurobiology: by explicitly constructing completions of images, we will be able to provide testable hypotheses for neurobiological function of V1.

2. Modeling V1 via the roto-translation group

In this section, we review the basic biological findings describing the function of V1 and describes a mathematical model of V1. Moreover, we describe the connection,

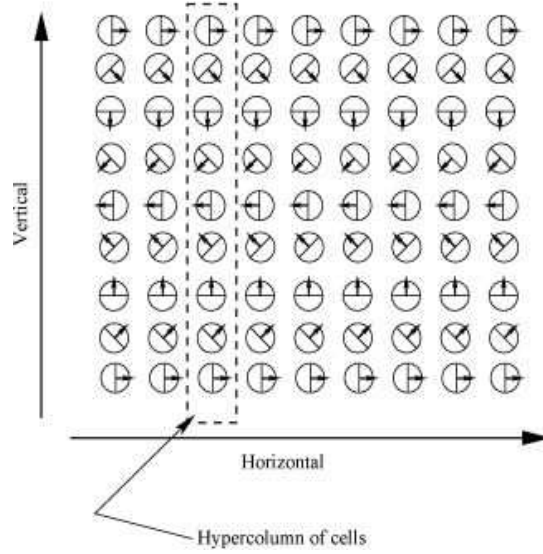


Fig. 1. A schematic of the structure of V1

provided by Citti and Sarti⁵, between minimal surfaces in the model space and solutions to the problem of amodally completing regions of occluded image data.

Over the past several decades, the function and operation of the first layer of the visual cortex, V1, has become increasingly clear. Early research showed that V1 contains so-called simple cells that are sensitive to, among other things, brightness gradients with a particular orientation. These cells are arranged in columns sharing the same orientation preference^{14,15} and the columns are arranged in hypercolumns which represent all possible orientations. This view was further explored and modeled mathematically,^{13,23} where the authors modeled the hypercolumnar cell structure using a contact manifold. The contact model is based on a simplifying assumption that treats each column as a point, ignoring the column structure to focus on the hypercolumn structure. Mathematically, they use the manifold $\mathbb{R}^2 \times \mathbb{S}^1$ to model the hypercolumn structure by placing a circle of directions above each point $(x, y) \in \mathbb{R}^2$. Each point (x, y, θ) represents a column of cells associated to an (x, y) point of retinal data, all of which are attuned to the orientation give by the angle θ . See figure 1 for a schematic of the hypercolumnar structure.

Early assumptions that cortical connectivity should run mostly vertically along the hypercolumns and be severely restricted in horizontal directions, while supported by some research, was contradicted by later evidence which showed that there is “long range horizontal” connectivity in the cortex. These experiments (see for example, Gilbert et al¹⁰) indicated that horizontal connections are made between cells in different hypercolumns of similar orientation preference. Moreover,

experimental evidence showed that there is a stronger preference for communication between cells of not only similar orientation preference but for ones that lie (roughly) along the axis corresponding to the shared orientation. In other words, using the notation of the above model, if (x, θ) and (y, θ) are points in different hypercolumns with the same angle preference θ , communication between the cells is preferred if the direction θ corresponds with the direction of the vector from x to y in \mathbb{R}^2 . This evidence points towards a geometric structure in this layer where communication between adjacent cells is allowable in certain directions, vertically and between cells in different hypercolumns of similar orientation sensitivity, and vastly restricted in all other directions. This type of situation has been studied in a variety of settings including, for example, control theoretic problems where the degrees of freedom at a particular point are restricted.

Petitot and Tondut^{22, 23} incorporate these biological findings into their model by introducing a contact structure on $\mathbb{R}^2 \times \mathbb{S}^1$ via the one form $\omega = dx - \theta dy$ and introduce a sub-Riemannian metric associated to the contact two-plane distribution to encode the geometry of the model of V1. The plane field given by the kernel of ω , $\text{span}\{\partial_\theta, \partial_y + \theta \partial_x\}$, corresponds to the space of allowable directions at each point. Notice that these are precisely the vertical direction and the direction which links cells in different hypercolumns with the same θ value. Citti and Sarti⁵ use the following explicit realization of the roto-translation group, \mathcal{RT} :

- \mathcal{RT} is diffeomorphic to $\mathbb{R}^2 \times \mathbb{S}^1$ with coordinates (x, y, θ) .
- The following three vector fields span the tangent space at each point:

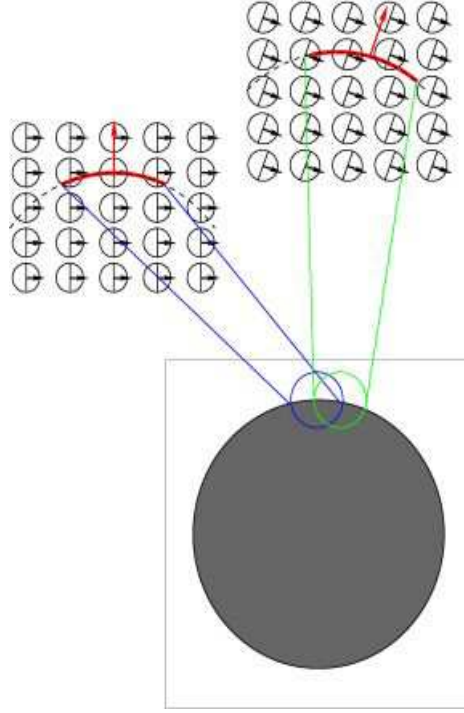
$$\begin{aligned} X_1 &= \cos(\theta) \frac{\partial}{\partial x} + \sin(\theta) \frac{\partial}{\partial y} \\ X_2 &= \frac{\partial}{\partial \theta} \\ X_3 &= -\sin(\theta) \frac{\partial}{\partial x} + \cos(\theta) \frac{\partial}{\partial y} \end{aligned} \tag{2.1}$$

We note that $[X_2, X_1] = X_3$ and $[X_2, X_3] = -X_1$.

- For an image $I : D \subset \mathbb{R}^2 \rightarrow \mathbb{R}$, its representation, $\Sigma(I)$, in \mathcal{RT} is given by $(x, y, \theta(x, y))$ where $(x, y) \in D$ and θ is given by

$$\frac{\nabla I}{|\nabla I|} = (-\sin(\theta), \cos(\theta))$$

We note that this is an explicit realization of the model described above and matches with the biological evidence concerning horizontal connectivity. The contact subbundle in this presentation is simply $\text{span}\{X_1, X_2\}$. It is a direct calculation that this subbundle gives a contact structure and, placing an inner product on this subbundle making $\{X_1, X_2\}$ orthonormal, we have a standard sub-Riemannian metric on \mathcal{RT} (see the next section for a precise definition). One of the main contributions of Citti and Sarti's adaptation of the cortical model is the use of an explicit lifting

Fig. 2. Example of lifting an image to \mathcal{RT}

function that transforms retinal data into a surface in the cortex and allows direct use of the Carnot-Carathéodory structure.

To explore this further, we investigate the application of the model to an image. Using the representation above, we see that the direction given by the angle $(\cos(\theta), \sin(\theta))$ points in a direction perpendicular to the gradient of I , i.e. a direction tangent to the level sets of I . Thus, if nearby points have the same intensity and thereby lie on the same level sets of I , their θ representations will be the same. As θ denotes a position in a hypercolumn of cells over the point (x, y) , this echoes the biological finding horizontal communication occurs between cells of similar orientation specificity and the property that the representation respects level lines reflects the biological principle that communication between point (x_0, y_0, θ) and (x_1, y_1, θ) is permitted if θ points in the same direction as the vector from (x_0, y_0) to (x_1, y_1) . In figure 2, we give a schematic of lifting a simple image to \mathcal{RT} . Represented are two layers of cells of similar orientation preference but different hypercolumns and two sections of the image that could plausibly be lifted to those layers.

Citti, Sarti and Manfredini⁴ provide a link between mean curvature flow in Rie-

mannian approximates of the sub-Riemannian space and the celebrated Mumford-Shah functional. Further, Citti and Sarti⁵ provided a link between the flow mechanism and several other models including elastica methods¹⁹ and the Ambrosio-Masnou model¹. Moreover, they showed that surfaces that were asymptotically stationary under the flows in the Riemannian approximates to \mathcal{RT} are minimal surfaces in the sub-Riemannian roto-translation group. As discussed in the introduction, minimal surfaces in Carnot-Carathéodory spaces have been examined in some generality^{7,8,12} as well as in more restricted settings.^{2,3,9,20,21}

Citti and Sarti⁵ use the model of V1 to investigate the problem of amodally filling in an image when a portion of the image is missing due to occlusion or some other factor. To use the model, Citti and Sarti took image data with a portion deleted and used an approximation of the flow described above to find a minimal spanning surface that “fills” the hole in the image. In other words, they find solutions to the minimal surface problem subject to Dirichlet boundary conditions. In the next sections, we will examine the minimal surface problem in the setting of a class of sub-Riemannian spaces which include the roto-translation group. The main goal of this paper is to provide a description of such minimal surfaces and to describe method by which they can be constructed in particularly a simple manner.

3. Notation

In this section, we fix the basic notation used throughout the paper. Let \mathcal{G} be a topologically three dimensional one step graded Lie group. In other words, the Lie algebra of left invariant vector fields \mathcal{V} splits as

$$\mathcal{V} = \mathcal{V}_0 \oplus \mathcal{V}_1, \quad \dim \mathcal{V}_0 = 2, \quad \mathcal{V}_1 = [\mathcal{V}_0, \mathcal{V}_0]$$

Moreover, we assume the following

- \mathcal{G} is equipped with a Riemannian metric g , which we sometimes denote in inner product notation by $\langle \cdot, \cdot \rangle$ and which makes the grading orthogonal.
- ∇^{LC} is the Levi-Civita connection associated to g
- *Assumption 1:* \mathcal{G} is said to satisfy assumption 1 if

$$[\mathcal{V}_0, \mathcal{V}_1] \subset \mathcal{V}_0$$

- We define a Carnot-Carathéodory distance on \mathcal{G} by

$$d_{cc}(x, y) = \inf_{\gamma \in \mathcal{A}} \left\{ \int \langle \gamma', \gamma' \rangle^{\frac{1}{2}} \mid \gamma(0) = x, \gamma(1) = y \right\}$$

where \mathcal{A} is the set of all absolutely continuous paths that, where their derivatives are defined, have $\gamma' \in \mathcal{V}$.

We note that if \mathcal{G} is nilpotent, then G is known as a *Carnot group*. We review two special examples.

Example 3.1. *The Heisenberg group.* The topologically three dimensional Heisenberg group, \mathbb{H} , is one of the simplest nonabelian nilpotent Lie groups. As a smooth

manifold, it is diffeomorphic to \mathbb{R}^3 . Using the terminology above, we have the Lie algebra given as

$$\mathfrak{h} = \mathcal{V}_0 \oplus \mathcal{V}_1$$

with $\mathcal{V}_0 = \text{span}\{X_1, X_2\}$ and $\mathcal{V}_1 = \text{span}\{X_3\}$ where there is a single nontrivial bracket operation, $[X_1, X_2] = X_3$. We note that, as \mathbb{H} is nilpotent, it is a Carnot group.

Example 3.2. *The Roto-Translation group.* As the roto-translation group, \mathcal{RT} , appears centrally in the model of visual processing in V1, we review its abstract structure. As a smooth manifold, it is diffeomorphic to $\mathbb{R}^2 \times \mathbb{S}^1$ and, using the terminology above, we have the Lie algebra given as

$$\mathfrak{h} = \mathcal{V}_0 \oplus \mathcal{V}_1$$

with $\mathcal{V}_0 = \text{span}\{Y_1, Y_2\}$ and $\mathcal{V}_1 = \text{span}\{Y_3\}$ where we have the following nontrivial bracket operations, $[Y_1, Y_2] = Y_3, [Y_2, Y_3] = Y_2$. Equation (2.1) in section 2 give a particular presentation of \mathcal{RT} . We note that \mathcal{RT} is not a Carnot group as it is not nilpotent.

Given a submanifold $S \subset \mathcal{G}$, the sub-Riemannian geometry of S is determined by the *horizontal normal* to S , N_0 , which is simply the projection of the Riemannian normal, N , to \mathcal{V}_0 , the first layer of the grading. Explicitly, if $\{X_1, X_2, X_3\}$ is a left invariant orthonormal basis of $T\mathcal{G}$ with $\mathcal{V}_0 = \text{span}\{X_1, X_2\}$ and S is given as a level set $\varphi = 0$ then,

$$\begin{aligned} N_0 &= \text{proj}_{\mathcal{V}_0} N \\ &= \text{proj}_{\mathcal{V}_0} ((X_1 \varphi) X_1 + (X_2 \varphi) X_2 + (X_3 \varphi) X_3) = (X_1 \varphi) X_1 + (X_2 \varphi) X_2 \end{aligned}$$

We also define the *unit horizontal normal*:

$$\nu = \frac{N_0}{\langle N_0, N_0 \rangle^{\frac{1}{2}}}$$

Minimal surfaces in Carnot-Carathéodory spaces have been investigated in a number of settings^{2, 3, 7–9, 12, 20, 21}. In particular, Danielli, Garofalo and Nheieu⁷ show that a C^2 hypersurface in a Carnot group G satisfy the following minimal surface equation:

$$\text{div}_0 \nu = 0$$

where div_0 is the horizontal divergence operator on \mathcal{V} . As shown in the next two sections, this equation also characterizes minimal surfaces in the class of groups described above which satisfy assumption 1.

4. Minimal surfaces in \mathcal{RT}

Lemma 4.1. *If \mathcal{G} satisfies assumption 1, i.e.*

$$[\mathcal{V}_0, \mathcal{V}_1] \subset \mathcal{V}_0 \quad (4.1)$$

then there exists a global strictly pseudoconvex pseudohermitian structure (η, J, \mathcal{G}) with the following properties

- $H = \text{span } \mathcal{V}_0$ is the contact distribution for η .
- $V = \text{span } \mathcal{V}_1$ is spanned by the characteristic vector field T for η .
- The Levi metric agrees with g on H and is conformal with constant scaling factor to g on V .

Proof: Let X_1 and X_2 be a left invariant orthonormal frame for \mathcal{V}_0 and set $T = [X_1, X_2] \in \mathcal{V}_1$. By left invariance and the bracket generating property of \mathcal{V}_0 , we see that X_1, X_2, T form a global orthonormal frame for $T\mathcal{G}$. Set η to be the dual 1-form for T with respect to this frame. Then clearly $H = \text{Ker } \eta$ and strict pseudoconvexity is immediate as H bracket generates at 1-step. The additional bracket condition (4.1) implies that $T \lrcorner d\eta = 0$. Thus the first two properties hold automatically regardless of which complex structure J is chosen for H .

Define $J : \mathcal{V}_0 \rightarrow \mathcal{V}_0$ by $JX_1 = -X_2$ and $JX_2 = X_1$. Next we extend J to all of $T\mathcal{G}$ by setting $JT = 0$ and declaring J to be linear over \mathbb{R} . The Levi metric defined by

$$h(X, Y) = d\eta(X, JY) + \eta(X)\eta(Y)$$

then clearly is compatible with g in the required fashion. ■

In this setting, we can now employ the techniques of pseudohermitian and CR geometry. Our key tool is the existence of a canonical connection ∇ , derived independently by Webster²⁶ and Tanaka²⁵, for any strictly pseudoconvex pseudohermitian geometry. The defining properties of the connection are as follows:

- $H, T, \eta, d\eta$ and J are all parallel.
- $\text{Tor}(X, Y) = d\eta(X, Y)T$ for $X, Y \in H$.
- $\text{Tor}(JX, T) = J\text{Tor}(X, T) \in H$ for $X \in H$.

Computations using this connection are most easily conducted in the moving frame approach of Cartan, adapted to this setting by Webster²⁶. For this technique, we first complexify the contact distribution H and define the space of $(1, 0)$ and $(0, 1)$ vector fields to be the $+i$ and $-i$ eigenspace of J respectively. The $(1, 0)$ vector fields are then spanned by

$$Z = X_2 - iX_1.$$

The vector fields Z, \bar{Z} and T then form an orthonormal (complex) frame for the complexified tangent space. The dual frame will be denoted by $\zeta, \bar{\zeta}$ and η . We

introduce the connection form ω via the identity

$$\nabla Z = \omega \otimes Z.$$

With respect to our frame the Webster-Tanaka connection and Levi metric can be uniquely computed from the following equations²⁶:

- $d\eta = ih\zeta \wedge \bar{\zeta}$.
- $dh = \omega h + h\bar{\omega}$.
- $d\zeta = \zeta \wedge \omega + \eta \wedge \tau$.
- $\tau = 0 \bmod \bar{\zeta}$.

The 1-form τ is known as the torsion form.

This connection proves well adapted to many geometric problems. For the study of horizontally minimal surfaces we have the following theorem.

Theorem 4.1. *Suppose S is a non-characteristic surface patch in a Carnot group satisfying our structure conditions. The horizontal minimal surface equation for S*

$$\operatorname{div} \nu = 0 \tag{4.2}$$

can be written as

$$\nabla_{J\nu} J\nu = 0$$

where ν is the horizontal unit normal. Thus if S satisfies (4.2) then S is ruled by horizontal ∇ -geodesics.

Proof: The volume form for the Levi metric is given by $dV = \eta \wedge d\eta$. By the defining properties of the pseudohermitian structure this is a constant multiple of the Riemannian volume form. From this we immediately see that dV is parallel for ∇ and the divergence operator for dV agrees with the Riemannian divergence. Further it follows that $T \lrcorner \eta \wedge d\eta = d\eta$ and so

$$\operatorname{div} T = 0.$$

Now ν , $J\nu$ and T form a local orthonormal frame for $T\mathcal{G}$. A standard formula in Riemannian geometry (see for example Kobayashi¹⁶) then yields

$$\operatorname{div} X = \operatorname{trace}(\nabla X + \operatorname{Tor}(X, \cdot)).$$

If X is horizontal then the second part of the trace formula vanishes identically by the defining properties of the Webster-Tanaka connection. Using our particular choice of frame we then see that

$$\begin{aligned} \operatorname{div} \nu &= \langle \nabla_\nu \nu, \nu \rangle + \langle \nabla_{J\nu} \nu, J\nu \rangle + \langle \nabla_T \nu, \nu \rangle \\ &= -\langle \nu, \nabla_{J\nu} J\nu \rangle \end{aligned}$$

as the second and third terms vanish because H is parallel and the connection is metric respectively. Thus on a non-characteristic, horizontally minimal surface patch we have

$$\nabla_{J\nu} J\nu = 0 \tag{4.3}$$

everywhere. The integral curves of $J\nu$ are therefore ∇ -geodesics. But $J\nu$ spans the intersection of TS with H . Thus the integral curves of $J\nu$ foliate S . ■

Remark 4.2. The divergence form of the minimal surface equation in \mathcal{RT} was first shown by Citti and Sarti⁵ (see section 2.9 proposition 3.1 of that paper) but is also a consequence of the more general psuedohermitian framework of Cheng, Huang, Malchiodi and Yang³. We also note that a version of this theorem, showing that smooth minimal surfaces are ruled, was first shown in section 2 of Cheng, Huang, Malchiodi and Yang,³ again in the more general context of psuedohermetian manifolds. We include the proof here for completeness and because it facilitates the computations below.

We shall now apply these techniques to the special case to the roto-translation group \mathcal{RT} . Here the underlying manifold is $\mathbb{R}^2 \times \mathbb{S}^1$ and \mathcal{V}_0 is defined by setting

$$X_1 = \cos \theta \frac{\partial}{\partial x} + \sin \theta \frac{\partial}{\partial y}, \quad X_2 = \frac{\partial}{\partial \theta}$$

and declaring them to be a left-invariant, orthonormal frame for a distribution H . The Riemannian structure by defining the transverse vector field,

$$T = [X_1, X_2] = \sin \theta \frac{\partial}{\partial x} - \cos \theta \frac{\partial}{\partial y}$$

and declaring it to be unit length and orthogonal to X_1 and X_2 . The remaining commutation relations can then be explicitly computed as

$$[X_1, T] = 0, \quad [X_2, T] = X_1.$$

When we run through the construction of Lemma 4.1 we note that g is exactly the Levi metric in this case. The contact form can be explicitly computed as

$$\eta = \sin \theta dx - \cos \theta dy$$

and the dual to the complex vector field $Z = X_2 - iX_1$ is

$$\zeta = \frac{1}{2} (d\theta + i \cos \theta dx + i \sin \theta dy).$$

Straightforward computations then yield

$$\begin{aligned} d\eta &= \cos \theta d\theta \wedge dx + \sin \theta d\theta \wedge dy = 2i\zeta \wedge \bar{\zeta} \\ d\zeta &= \frac{i}{2} d\theta \wedge (-\sin \theta dx + \cos \theta dy) = -\frac{i}{2} \zeta \wedge \eta + \frac{i}{2} \eta \wedge \bar{\zeta}. \end{aligned}$$

The first identity also follows from the fact that the pseudohermitian structure was explicitly constructed to ensure that X_1 and X_2 were orthonormal. Since $h = 2$ we can immediately deduce from the 2nd Webster identity that the connection form ω is pure imaginary. Thus we can deduce that

$$\omega = -\frac{i}{2}\eta, \quad \tau = \frac{i}{2}\bar{\zeta}.$$

This implies that for the frame X_1, X_2, T the only non-trivial covariant derivatives are in the T direction. By examining the real and imaginary parts of the equation

$$\nabla_T Z = -\frac{i}{2}Z$$

we see $\nabla_T X_1 = \frac{1}{2}X_2$ and $\nabla_T X_2 = -\frac{1}{2}X_1$.

The horizontal ∇ -geodesics can be computed explicitly. Consider a curve $\gamma = (x, y, \theta)$. Thus

$$\dot{\gamma} = (\dot{x}, \dot{y}, \dot{\theta}) = (\dot{x} \cos \theta + \dot{y} \sin \theta)X_1 + \dot{\theta}X_2 + (\dot{x} \sin \theta - \dot{y} \cos \theta)T.$$

Thus if γ is a purely horizontal curve, we must have

$$\dot{x} \sin \theta - \dot{y} \cos \theta = 0.$$

Under this assumption, $D_t \dot{\gamma} = 0$ if and only if both $\dot{\theta}$ and $\dot{x} \cos \theta + \dot{y} \sin \theta$ are constant. We can then solve the equation

$$\begin{pmatrix} \sin \theta & -\cos \theta \\ \cos \theta & \sin \theta \end{pmatrix} \begin{pmatrix} \dot{x} \\ \dot{y} \end{pmatrix} = \begin{pmatrix} 0 \\ R_0 \end{pmatrix}$$

to obtain $\dot{x} = R_0 \cos \theta$, $\dot{y} = R_0 \sin \theta$.

- Case 1: $\dot{\theta} \neq 0$. Set $R = R_0/\dot{\theta}$, then

$$x = x_c + R \sin \theta$$

$$y = y_c - R \cos \theta$$

$$\theta = \theta_0 + \dot{\theta}t.$$

Here $x_c = x_0 - R \sin \theta_0$, $y_c = y_0 + R \cos \theta_0$.

- Case 2: $\dot{\theta} = 0$. Set $R = R_0$, then

$$x = x_0 + R(\cos \theta_0)t$$

$$y = y_0 + R(\sin \theta_0)t$$

$$\theta = \theta_0.$$

In the sequel we shall refer to the horizontal ∇ -geodesics (and connected subsets of them) as rules.

5. Missing data and amodal completion

We next turn to the problem of filling in missing image data. Image data may be missing for a number of reasons: one object occludes another, the existence of a “blind spot” in the retina or some other physiological failure. In terms of digital image processing, data corruption, noise or object occlusion can *de facto* create a domain of missing data.

Using the roto-translation model for the hypercolumn structure in V1 described above, image data is lifted to \mathcal{RT} and missing data is filled by solving the minimal surface problem for the given boundary data.⁵ Mathematically, if $D \subset \mathbb{R}^2$ is an

open domain where image data is missing, and $c \in \mathcal{RT}$ is the image of ∂D under the lift $\theta(x, y)$ defined in section 2, then we wish to find a minimal surface Σ so that $\partial\Sigma = c$. Moreover, as discussed in the previous two sections, a C^2 surface meeting these requirements must satisfy the equation:

$$\operatorname{div}_0 \nu = 0$$

where ν is the unit horizontal normal to Σ . Moreover, by theorem Theorem 4.1, Σ must be ruled by horizontal ∇ -geodesics. For the balance of the paper, we will consider the following problem:

Occlusion problem: Given a smooth curve, c , in \mathcal{RT} which is the lift of the boundary of an open domain in \mathbb{R}^2 , can we find a smooth minimal surface spanning c which is ruled by ∇ -geodesics?

As referenced in the previous sections, this type of problem has been studied before in a number of sub-Riemannian settings. In addition to the observation that minimal surfaces in some settings are ruled surfaces, there are a number of results further describing the nature of solutions to the minimal surface problem with Dirichlet boundary data. Among these results, it is important to note that, at least in the Heisenberg²⁰ and Martinet-type spaces⁶, there are obstructions to the existence of smooth minimal spanning surfaces, even if the spanned curve c has arbitrarily nice behavior. Moreover the second author demonstrates²¹ that solutions to the Dirichlet problem for ruled minimal surfaces need not be unique (however, Cheng, Huang, Malchiodi and Yang³ prove a uniqueness result for surface subject to certain constraints on the characteristic locus). Thus, as the roto-translation group is locally very much like the Heisenberg group, we should expect to see issues with both existence and uniqueness. In light of this suggestive evidence, we present a list of conditions, each stronger than the next, concerning a smooth minimal spanning surface Σ :

- (I) Σ exists
- (II) Condition I and any rule connecting two points of c projects to a curve in the interior of D
- (III) Condition II and the projection of Σ to D is surjective.
- (IV) Condition III and Σ is a graph over D
- (V) Condition IV and Σ is unique

We note that if condition II is violated, the rules, upon projection, would present potentially conflicting data for points exterior to D while if condition IV is violated, there would exist points interior to D with conflicting projected image data. Thus, condition III is sufficient to guarantee the existence of a completion of the image data (not just a spanning surface in \mathcal{RT}) although there may be conflicting data while IV would provide a completion with no conflicting data. However, as, *a priori*

there may be multiple lifts, only condition V would yield a unique completion of the image data.

The evidence cited above and the experimental evidence of multiple simultaneous completions of image data in \mathcal{RT}^5 suggests that we should not expect to be able to satisfy the more stringent requirements. As we develop the machinery to construct such surfaces, however, we will keep each of these conditions in mind.

6. Ruled surfaces in \mathcal{RT}

In this section, we begin the investigation of the existence and properties of minimal ruled spanning surfaces of curves in \mathcal{RT} . As we require the solution to the occlusion problem to be a surface ruled by ∇ -geodesics, we first look at the set of points which can be connected to a given point by ∇ -geodesics. With this in mind, we make the following definition:

Definition 6.1. For a point $p \in \mathcal{RT}$ we define the accessible set $\mathcal{A}(p)$ to be the collection of points that can be connected to p by a single, horizontal ∇ -geodesic.

Lemma 6.1. *Given a point $p = (x_0, y_0, \theta_0)$, the set of accessible points is given by the implicit equation*

$$\frac{y - y_0}{x - x_0} = \tan\left(\frac{\theta + \theta_0}{2}\right).$$

Proof: When the connecting ∇ -geodesic is a straight line this is immediate. The other case follows easily from the trigonometric identity

$$\tan\left(\frac{\theta + \theta_0}{2}\right) = \frac{\cos \theta_0 - \cos \theta}{\sin \theta - \sin \theta_0}. \quad (6.1)$$

The proof of this identity is an easy exercise with the tangent half-angle formulas. ■

This provides a description of the accessible set of p :

Lemma 6.2. *Every accessible set $\mathcal{A}(p)$ is the image of an embedding of the Möbius strip into \mathcal{RT} .*

Proof: We shall give two arguments for this result. One purely geometric, the other more analytic.

From Lemma 6.1 we note that each θ -slice of $\mathcal{A}(p)$ projects to a straight line in the (x, y) -plane of gradient $\tan((\theta + \theta_0)/2)$. As θ increases this line rotates spanning out a helicoid. However since we must identify $\theta = 2\pi$ with $\theta = 0$ and the factor of $1/2$ inside the tan means that there is an orientation switch at the join. Thus $\mathcal{A}(p)$ is a non-orientable line over \mathbb{S}^1 which therefore must be diffeomorphic to a Möbius strip.

A more analytic approach is to consider the ∇ -exponential map at p restricted to the horizontal distribution. From our explicit description of the horizontal geodesics

passing through p we note that if $p = (x_0, y_0, \theta_0)$ then

$$\begin{aligned} \exp_p(aX_1 + bX_2) = & (x_0 + a/b(\sin(\theta_0 + b) - \sin \theta_0), \\ & y_0 + a/b(\cos \theta_0 - \cos(\theta_0 + b)), \theta_0 + b) \end{aligned} \quad (6.2)$$

at least when $b \neq 0$. When $b = 0$ we instead get

$$\exp_p(aX_1) = (x_0 + a \cos \theta_0, y_0 + a \sin \theta_0, \theta_0). \quad (6.3)$$

If $\exp(a, b) = \exp(a', b')$ we must therefore have that $b = b' + 2k\pi$ (with neither being 0) and $a'/b' = a/b$. This later can be summarized as the points (a, b) and (a', b') must lie on the same line through the origin with $b = b' + 2k\pi$. Therefore the exponential map is bijective from $\mathbb{R} \times [-\pi, \pi]$ to $\mathcal{A}(p)$ provided that the sides of the strip are identified via $(a, -\pi) \sim (-a, \pi)$. This provides an explicit embedding of the Möbius strip into \mathcal{RT} with image $\mathcal{A}(p)$. ■

For each point on a curve γ , $\mathcal{A}(\gamma(t))$ may contain many points of γ or very few. Of most interest to the question of building spanning surfaces are the points $\gamma(t)$ where $\gamma \cap \mathcal{A}(\gamma(t)) = \{\gamma(t)\}$ - i.e. the points that only connect to themselves. These points give constraints on the formation of a minimal ruled spanning surface. To help understand these points, we make the following definition:

Definition 6.2. Given an embedded curve γ and a point $p \in \gamma$ we define

$$\mathcal{A}(p, \gamma) = \gamma \cap \mathcal{A}(p),$$

the points in γ accessible to p . A point p such that $\mathcal{A}(p, \gamma) = \{p\}$ is called an solitary point of γ . The solitary points of γ will be denoted $\mathcal{S}(\gamma)$. A point $p = \gamma(t)$ such that $\dot{\gamma} \in H$ is called a Legendrian point of γ . The Legendrian points of γ will be denoted $\mathcal{L}(\gamma)$. We also define the orthogonal points of γ , denoted $\mathcal{O}(\gamma)$ to be where $\dot{\gamma} \in \text{span}\{X_1, X_3\}$.

As seen in the definition, there are two types of solitary points, the Legendrian points and the non-Legendrian points. We remark that for a Legendrian point p , the candidate rule passing through p is tangent to the curve γ and, as in the Heisenberg group²⁰, one can use this as a starting place for building a ruled minimal spanning surface. the non-orientability of the accessible sets in the roto-translation case means that unlike for the Heisenberg group we cannot deduce that all solitary points are Legendrian. Indeed non-Legendrian solitary points present more of a problem as the candidate rules will be transverse at such a point. To investigate the structure of the set of solitary points further we prove the following lemma.

Lemma 6.3. *For any embedded curve γ , the set $\mathcal{S}(\gamma) - \mathcal{L}(\gamma)$ is open.*

Proof: If $p \in \mathcal{S}(\gamma) - \mathcal{L}(\gamma)$, then γ intersects $\mathcal{A}(p)$ only at p and does transversely. A small perturbation of the base point p will cause a small perturbation of the Möbius strip embedding. As γ is transverse to $\mathcal{A}(p)$, a small perturbation of p cannot increase the number of nearby intersections. Away from p the Euclidean

distance of γ from $\mathcal{A}(p)$ can be uniformly bounded below and so a small perturbation will not introduce any distant intersections. Thus curve points sufficiently near to p will also be solitary. Clearly they will also be non-Legendrian. ■

Lemma 6.4. *Suppose γ is an embedded curve and $\gamma(0) \in \mathcal{J}(\gamma) - \mathcal{L}(\gamma)$. Then the map*

$$\begin{aligned}\Theta : \mathbb{S}^1 &\rightarrow \mathbb{S}^1 \\ t &\mapsto \theta(\gamma(t))\end{aligned}$$

is surjective.

Proof: This is a topological argument. Suppose γ is a curve in \mathcal{RT} that projects to the xy-plane bounding a domain D . Further suppose there exists $\theta_0 \in \mathbb{S}^1$ not in the image of Θ . Then, there exists a neighborhood of θ_0 , N_0 , so that $N_0 \cap \text{Im}(\Theta) = \emptyset$. By Lemma 6.2, $\mathcal{A}(\gamma(0))$ is a Möbius strip. However $\mathcal{A}_0(\gamma(0)) := \mathcal{A}(\gamma(0)) \setminus (\mathbb{R}^2 \times N_0)$ is orientable. Since γ , by assumption, cannot enter $\mathbb{R}^2 \times N_0$ we see that γ lies to one side of $\mathcal{A}_0(\gamma(0))$. However, since $\gamma(0) \in \mathcal{J}(\gamma) - \mathcal{L}(\gamma)$, γ must intersect $\mathcal{A}_0(\gamma(0))$ transversely at $\gamma(0)$. This is a contradiction. ■

For the occlusion problem we shall work exclusively with curves that occur as the boundary of a smooth, simply connected region D lifted by the contour direction field of an intensity function $I : \mathbb{R}^2 \rightarrow \mathbb{R}$. The boundary ∂D is can be viewed as the image of an embedding $\beta : \mathbb{S}^1 \rightarrow \mathbb{R}^2$. Away from critical points of I , we can define the lifting function $\theta : \mathbb{S}^1 \rightarrow \mathbb{S}^1$ by

$$\theta(t) = \arctan \left(-\frac{I_x \circ \beta(t)}{I_y \circ \beta(t)} \right)$$

where at each point we choose the branch of \arctan which makes θ continuous. We shall that an occlusion is *non-degenerate* if the number of critical points of I lying inside ∂D is finite and θ can be extended continuously across each critical point. The occlusion is *completely non-degenerate* if there are no critical points on the boundary. Using this function θ we construct the curve $\gamma = (\beta, \theta)$. In addition we define the normal angle function for β by

$$\frac{\beta'(t)}{|\beta'(t)|} = (-\sin \varphi_\beta(t), \cos \varphi_\beta(t)).$$

From these we construct the *transversality function* for γ ,

$$Q(t) = \theta(t) - \varphi_\beta(t).$$

From the definitions, it is clear that a non-critical point $\gamma(t)$ is Legendrian if and only if $Q(t) = \pi/2 + k\pi$, $k \in \mathbb{Z}$. Likewise $\gamma(t)$ is orthogonal if and only if $Q(t) = k\pi$. We record this and another fact in a lemma:

Lemma 6.5. *For any lift γ associated to a completely non-degenerate occlusion problem,*

18 *Robert K. Hladky and Scott D. Pauls*

- (1) $\gamma(t)$ is Legendrian if and only if $Q(t) = \frac{\pi}{2} + k\pi$ for some integer k .
- (2) $\gamma(t)$ is orthogonal if and only if $Q(t) = k\pi$ for some integer k .
- (3) $\mathcal{L}(\gamma)$ is non-empty.

Proof: For the first item, we note that, by definition, γ is Legendrian if $\gamma' \in H$. Computing, we have

$$\langle \gamma'(t), X_3 \rangle = \beta'(t) \cdot (\nabla I) = |\beta'(t)|(\cos(\theta(t) - \varphi_\beta(t))) = |\beta'(t)| \cos(Q(t))$$

and so, if we assume $\gamma(t)$ is Legendrian, we have that, equivalently, $\beta'(t) \cdot \nabla I = 0$ or $Q(t) = \theta(t) - \varphi_\beta(t) = \frac{\pi}{2} + k\pi$. The second item, concerning orthogonal points, follows in the same way.

The last item follows immediately from the observation that

$$\int_{\partial D} \nabla I \cdot d\vec{r} = \int_0^{2\pi} |\nabla I(\beta(t))| |\beta'(t)| \cos \alpha = 0$$

where α is the angle between ∇I and β' . Since the first two terms of the integral are strictly positive we must have $\cos \alpha$ taking both positive and negative values. In particular, this implies there are at least two points in $[0, 2\pi)$ where $\cos(\alpha) = 0$. By the computation at the outset of the proof, these two points are Legendrian points. ■

Remark 6.3. We note that in the proof, we provide a geometric interpretation of Q : it measures the angle between β' and ∇I .

7. Occluded Disks

For computational reasons, it is useful to restrict attention to curves γ that are lifts of circles in \mathbb{R}^2 to the rototranslation group. The lifts we are most interested in come from the direction angles of the contours of an intensity plot which has an ambiguity associated with the choice of orientation. Given a point (x, y) and a contour passing through this point at angle θ , it is unclear whether to lift it to (x, y, θ) or $(x, y, \theta + \pi)$. Accordingly, for a point $p = (x, y, \theta) \in \mathcal{RT}$ we shall define its conjugate point to be $\bar{p} = (x, y, \theta + \pi)$ and frequently consider conjugate lifts γ and $\bar{\gamma}$ simultaneously.

Any circular lift γ can be expressed parametrically in standard form as

$$\gamma(t) = (x_0 + R \cos t, y_0 + R \sin t, \theta(t)). \quad (7.1)$$

When γ is understood, we shall frequently refer to a point of $p \in \gamma$ simply by its parameter value with this parametrisation. With this parametrization understood we can simplify the transversality function Q to

$$Q(t) = \theta(t) - t. \quad (7.2)$$

Lemma 7.1. *For a circular lift $\gamma = (x, y, \theta)$, the non-trivial part of $\mathcal{A}(\gamma(t), \gamma)$ is given implicitly by*

$$Q(t) + Q(u) = (2k + 1)\pi, \quad k \in \mathbb{Z} \quad (7.3)$$

and $\mathcal{A}(\gamma(t), \bar{\gamma})$ is given implicitly by

$$Q(t) + Q(u) = 2k\pi, \quad k \in \mathbb{Z}. \quad (7.4)$$

Proof: From Lemma 6.1 we see that $\gamma(u) \in \mathcal{A}(t, \gamma)$ if and only if

$$\frac{\sin u - \sin t}{\cos u - \cos t} = \tan \left(\frac{\theta(u) + \theta(t)}{2} \right).$$

Applying the trigonometric identity (6.1) we see that this is equivalent to

$$\cot \left(\frac{u + t}{2} \right) = \tan \left(\frac{\theta(u) + \theta(t)}{2} \right).$$

The result then follows easily from standard arguments in trigonometry. A virtually identical arguments yields the second part also. ■

Lemma 7.2. *Conjugation twist-commutes with the exponential map in the sense that.*

$$\exp_{\bar{p}}(a, b) = \overline{\exp_p(-a, b)}.$$

Proof: This follows from direct computation from (6.2) and (6.3). ■

Corollary 7.1. *If $\bar{q} \in \mathcal{A}(p)$ then $q \in \mathcal{A}(\bar{p})$. Furthermore the projections to \mathbb{R}^2 of the connecting rules match precisely.*

Therefore when connecting points obtained from lifting intensity plots we need only consider how points in γ can be connected to either γ or $\bar{\gamma}$. We shall write $t \sim u$ if either $\gamma(u)$ or $\bar{\gamma}(u)$ lies inside $\mathcal{A}(\gamma(t))$.

Lemma 7.3. *The Legendrian points of γ occur precisely where*

$$Q(t) = \pi/2 + k\pi, \quad k \in \mathbb{Z}.$$

The orthogonal points of γ occur precisely where

$$Q(t) = k\pi, \quad k \in \mathbb{Z}.$$

Proof: Since γ is parametrized by (7.1), we can explicitly compute that

$$\begin{aligned} \dot{\gamma} &= -R \sin(t) \frac{\partial}{\partial x} + R \cos(t) \frac{\partial}{\partial y} + \dot{\theta} X_2 \\ &= R \sin(\theta - t) X_1 + R \cos(\theta - t) X_3 + \dot{\theta} X_2. \end{aligned}$$

For $\gamma(t) \in \mathcal{L}(\gamma)$ it is then necessary and sufficient that $\cos(\theta - t) = 0$. For $\gamma(t) \in \mathcal{O}(\gamma)$ the condition becomes $\sin(\theta - t) = 0$. The result follows easily. ■

Corollary 7.2. $\overline{\mathcal{L}(\gamma)} = \mathcal{L}(\bar{\gamma})$, $\overline{\mathcal{O}(\gamma)} = \mathcal{O}(\bar{\gamma})$.

Corollary 7.3. *On an implicit plot of all points (t, u) such that $t \sim u$. Any transverse crossing of the leading diagonal $u = t$ occurs at either a Legendrian or an orthogonal point.*

Corollary 7.4. *If $t \sim u$ and $\gamma(t) \in \mathcal{L}(\gamma)$ then $\gamma(u) \in \mathcal{L}(\gamma)$. Furthermore, the connecting rule projects to the same circle as γ .*

If $t \sim u$ and $\gamma(t) \in \mathcal{O}(\gamma)$ then $\gamma(u) \in \mathcal{O}(\gamma)$.

With circular lifts, if two points on γ are known to be connectable then it is a straightforward matter to explicitly describe the connecting rule. If $(x_0, y_0, \theta_0) \sim (x_1, y_1, \theta_1)$ with $\theta_0 \neq \theta_1$ then the connecting rule must have the parametrisation $(x_c + R \sin \varphi, y_c - R \cos \varphi, \varphi)$. Thus we need only solve the matrix equation

$$\begin{pmatrix} 1 & 0 & \sin \theta_0 \\ 0 & 1 & -\cos \theta_0 \\ 1 & 0 & \sin \theta_1 \\ 0 & 1 & -\cos \theta_1 \end{pmatrix} \begin{pmatrix} x_c \\ y_c \\ R \end{pmatrix} = \begin{pmatrix} x_0 \\ y_0 \\ x_1 \\ y_1 \end{pmatrix} \quad (7.5)$$

where the fact that the points are connectable guarantees the existence of a solution. Elementary methods yield that generically

$$R = \frac{x_1 - x_0}{\sin \theta_1 - \sin \theta_0}, \quad x_c = x_0 - R \sin \theta_0, \quad y_c = y_0 + R \cos \theta_0. \quad (7.6)$$

This of course yields two separate connecting rule segments depending on whether φ transverses \mathbb{S}^1 clockwise or anticlockwise.

Lemma 7.4. *If γ is the circular boundary of a completely nondegenerate occlusion and if $R(t) = R(\gamma(t))$, then $R \neq 0$.*

Proof: We may assume, without loss of generality, that $(x_0, y_0, \theta_0) = (0, 0, 0)$, $\gamma(0) = (x_0, y_0)$ and γ is parameterized by arclength. If R is zero, then we must have that (x_0, y_0, θ_0) is connected to itself. Thus, there exists a finite speed parametrization $(c_1(t), c_2(t))$ so that $(c_1(0), c_2(0)) = (0, 0)$ and $(\gamma_1(c_1(t)), \gamma_2(c_2(t)))$ is connected to $\gamma(t)$ for t close to 0. Using (7.5), if we let $R(t)$ be the radius of the circle connecting $(\gamma_1(c_1(t)), \gamma_2(c_2(t)))$ to $\gamma(t)$, for a generic choice of t , we must have

$$R(t) = \frac{\gamma_2(c_2(t)) - \gamma_2(t)}{\cos(\theta(c_2(t))) - \cos(\theta(t))} = -\frac{\gamma_1(c_1(t)) - \gamma_1(t)}{\sin(\theta(c_1(t))) - \sin(\theta(t))}$$

Assuming that $R \rightarrow 0$ as $t \rightarrow 0$, then we must have that

$$\begin{aligned} R(t) &= \lim_{t \rightarrow 0} \frac{\dot{\gamma}_2(c_2(t))\dot{c}_2(t) - \dot{\gamma}_2(t)}{\sin(\theta(c_2(t)))\dot{\theta}(c_2(t))\dot{c}_2(t) - \sin(\theta(t))\dot{\theta}(t)} \\ &= \lim_{t \rightarrow 0} \frac{\dot{\gamma}_1(c_1(t))\dot{c}_1(t) - \dot{\gamma}_1(t)}{\cos(\theta(c_1(t)))\dot{\theta}(c_1(t))\dot{c}_1(t) - \cos(\theta(t))\dot{\theta}(t)} = 0 \end{aligned}$$

As \sin, \cos, \dot{c}_i are bounded and $|\dot{\gamma}| = 1$, we have that $\dot{\theta} \rightarrow \pm\infty$ as $t \rightarrow 0$. However, direct computation shows that

$$\dot{\theta}(t) = -\frac{1}{|\nabla I|} \begin{pmatrix} -\frac{I_x}{|\nabla I|} \\ \frac{I_y}{|\nabla I|} \end{pmatrix} \mathcal{H} \begin{pmatrix} \cos(t) \\ -\sin(t) \end{pmatrix}$$

where \mathcal{H} is the Hessian of I . If $I \in C^2$ and the occlusion is completely nondegenerate, then $\dot{\theta}$ must be bounded on γ . Thus, R cannot tend to zero. ■

With these initial observations in place, we turn to the task of understanding when minimal spanning surfaces exist. We will investigate such surfaces using the following blueprint (if possible):

- (1) Construct the function Q as given in (7.2).
- (2) Find all solitary Legendrian points using lemma Lemma 7.3.
- (3) Starting from a solitary Legendrian points, construct connections between points on γ to other points on γ using the implicit equation

$$Q(t) + Q(u) = (2k + 1)\pi$$

and the matrix equation above.

Subject to goal of satisfying conditions II and III from section 5.

As we shall see, any one of these steps and/or goals may be violated. One issue we address first is that it may not always be possible to construct such a surface by connecting points of γ to other points of γ . In this case, as discussed above, it is natural to instead connect some (or all) points of γ to points of $\bar{\gamma}$.

8. The index of Q

To construct a minimal spanning surface for γ we choose the a Legendrian point as a starting place and attempt to build a monotone function $u(t)$ such that $u \sim t$ by following the branch of the implicit plot until we reach the other Legendrian point. If we implicitly differentiate either (7.3) or (7.4) with respect to t , we see that

$$u'(t) = \frac{\theta'(t) - 1}{1 - \theta'(u)} = -\frac{Q'(t)}{Q'(u)}.$$

In particular, these implicit plots fail to be graphs over the t -axis precisely when either $Q'(t) = 0$ or $Q'(u) = 0$. The presence of such points is a necessary condition for obstructions to the existence of a monotone function $u(t)$. If we have intervals of positive measure where $Q'(t)$ is strictly positive and others where it is strictly negative, then we note that a spanning surface will not be a graph over D as the change in sign forces the spanning surface to backtrack locally, violating our goal IV. Generically, even if such points occur we can still follow a branch of the implicit plot and construct connecting rules, however there will be non-uniqueness issues. This approach will only completely fail if the plot fails to be an embedded curve, which occurs only at points (t, u) where $Q'(t) = 0 = Q'(u)$.

If we can construct a monotone function $u(t)$, then the collection of connecting rules will form a minimal spanning surface for the lift γ . In practice, there are several types of obstructions to this method.

Of primary importance is the degree of the map $Q: \mathbb{S}^1 \rightarrow \mathbb{S}^1$. Since connections are made by implicitly solving the equation

$$Q(t) + Q(u) = \pi \pmod{2\pi} \tag{8.1}$$

the size of the set $\mathcal{A}(\gamma, t)$ is intimately related to $\deg Q$. For example if $\deg Q \neq 0$ then there cannot be any non-Legendrian solitary points as non-zero degree implies Q is surjective. Likewise, it is clear that

$$|\mathcal{L}(\gamma)| \geq 2 |\deg Q|.$$

Of course, critical points of Q add a separate pathology which influences the number of branches of the implicitly defined function u of (8.1).

For the occlusion problem, the degree of Q is directly related to the critical point theory of the intensity function $I(x, y)$. If the occlusion is completely non-degenerate, then there is a well-defined map

$$I_\theta = \frac{\nabla I}{|\nabla I|}: \partial D \cong \mathbb{S}^1 \rightarrow \mathbb{S}^1.$$

The continuous lift θ is then given by $I_\theta + \pi/2$. Hence

$$\deg Q = \deg I_\theta - 1.$$

To explore this further, we shall suppose that $I(x, y)$ has at most one (nearby) critical point p which if it exists is contained in the interior of the occluded region D . In this instance it follows from the definitions that

$$\deg Q = \text{index}_p \nabla I - 1$$

if p exists. If there is no critical point in the interior then I_θ extends to a continuous function on the interior disc. Standard results in algebraic topology then imply that $\deg I_\theta = 0$ and so $\deg Q = -1$.

Next, we examine various possibilities for the occlusion problem. We will deal primarily with completely nondegenerate curves.

8.1. Case 1: $\deg Q = -1$, $Q' \neq 0$

As a basic example, we consider the following example: set the intensity function as $I(x, y) = (1 + x^2(y - x)^2)^{-1}$ whose contour plot looks like an angled cross, see Figure 3. The region to be occluded is $(x - 2.4)^2 + (y - 2.6)^2 < 1$, which is over just one branch of the cross. While formally I has critical points everywhere along the lines $y = x$ and $x = 0$, we can replace I with $x(y - x)$ without altering the underlying contour plot. With this simplification, we have a completely non-degenerate occlusion with no occluded critical points. Thus $\deg Q = -1$ (and hence surjective onto \mathbb{S}^1). The implicit plot of (8.1) is shown in Figure 4. In this instance we see that Q is one-to-one from \mathbb{S}^1 to \mathbb{S}^1 and so there is only one branch of (8.1), which spans the entire range. Moreover, direct calculation shows that $Q'(t) \neq 0$ for all $t \in [0, 2\pi]$. The boundary lift γ has exactly 2 Legendrian points, represented in Figure 4 (b) by the intersection of the curve $Q(t)$ with the blue lines $Q = \pi/2$ and $Q = 3\pi/2$. The intersections with the lines $Q = 0, 2\pi$ and $Q = \pi$ correspond to the orthogonal points.

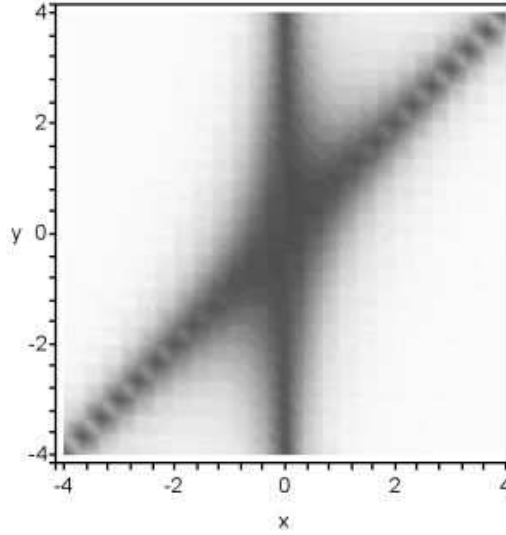
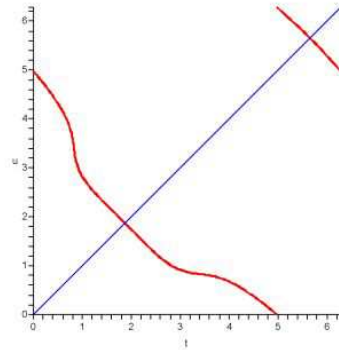
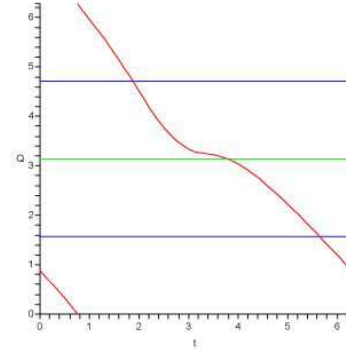
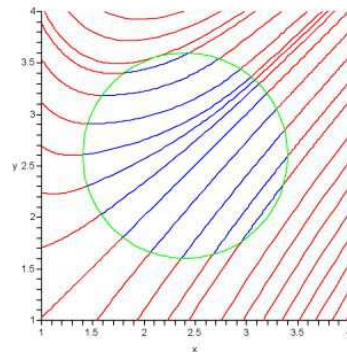


Fig. 3. Intensity plot for $I = (1 + x^2(x - y)^2)^{-1}$.

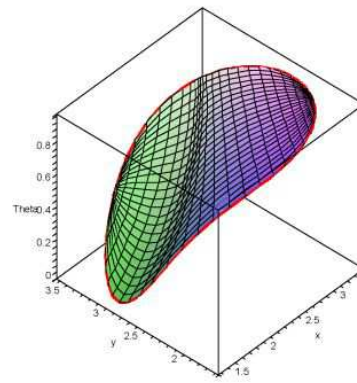
Since Legendrian points can only connect to other Legendrian points (by corollary Corollary 7.4), we see from the implicit plot of (8.1) that the Legendrian points for γ are solitary and correspond to the intersections with the leading diagonal in Figure 4 (a). Thus we can pick either and construct connecting rules by tracing the sole branch of the implicit plot until we reach the other Legendrian point. By symmetry every point on the curve has now been connected to another and we can build a surface ruled by the ∇ -geodesic segments that project into the interior of the occluded region. The projections of these segments provide a contour completion through the occluded region. In Figure 4 (c) and (d) we show the full contour completion together with the associated minimal lift in the roto-translation group. We note that it is possible to show that the surface constructed is a graph over the occluded region and hence satisfies condition IV.

8.2. Case 2: $\deg Q = -1$, Q' has zeros

The last example worked so well because not only was $\deg Q = -1$, but also because Q was injective. This was because the directions of the underlying contours were relatively uniform. If we move the occluded region in closer to the centre of the cross, we lose this uniformity and we find that Q despite having degree -1 is no longer injective. Examining Figure 5 confirms that there are points where $Q' = 0$ (this can also be confirmed by direct calculation). This is represented by the failure of the implicit plot of (8.1) to be a graph over either u or t . When we follow the program laid out earlier for constructing minimal spanning surfaces, we find that

24 *Robert K. Hladky and Scott D. Pauls*(a) $t \sim u$ (b) “ t vs Q ”

(c) Contour Completion



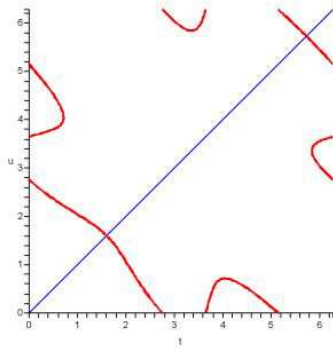
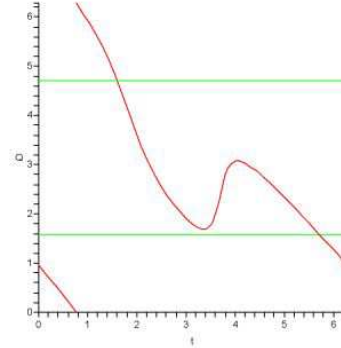
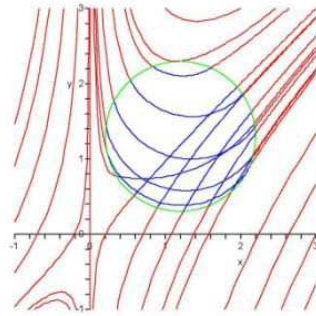
(d) Minimal Spanning Surface

Fig. 4. $I = (1 + x^2(x - y)^2)^{-1}$, Centre=(2.4, 2.6), Radius=1, Connecting γ to γ .

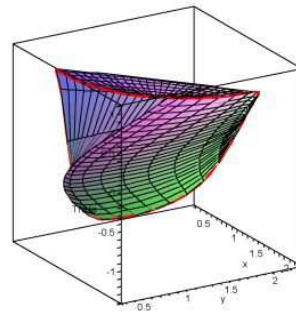
some points have multiple connections. The surface then connects to some parts of the curve as a ridge. Note this surface satisfies condition II but not III.

8.3. Case 3: $\deg Q = 0$

If $\deg Q = 0$ then there are possible obstructions to even local existence of spanning surfaces for γ . This phenomenon occurs due to the presence of non-Legendrian solitary points. Non-Legendrian solitary points do not occur in isolation but as open sets by Lemma 6.3. Since Q is continuous, the presence of non-Legendrian solitary points implies that the image of Q is contained in a narrow (width $< \pi$)

(a) $t \sim u$ (b) “ t vs Q ”

(c) Contour Completion



(d) Minimal Spanning Surface

Fig. 5. $I = (1 + x^2(x - y)^2)^{-1}$, Centre=(1.2, 1, 4), Radius=1, Connecting γ to γ .

band. In particular, this implies that the condition $\deg Q = 0$ is necessary. In the situation of a single critical point of I being occluded, the index of ∇I must be 1. In other words, we must be occluding a local maximum or minimum.

A simple example is to consider the circular lift

$$\gamma(t) = (\cos t, \sin t, t). \quad (8.2)$$

Here $Q(t) = 0$ everywhere and so every point is orthogonal with outward pointing orientation. The set of (t, u) that satisfy (8.1) is therefore empty. Every point is therefore solitary and non-Legendrian and there is no non-characteristic minimal surface that spans even a part of γ .

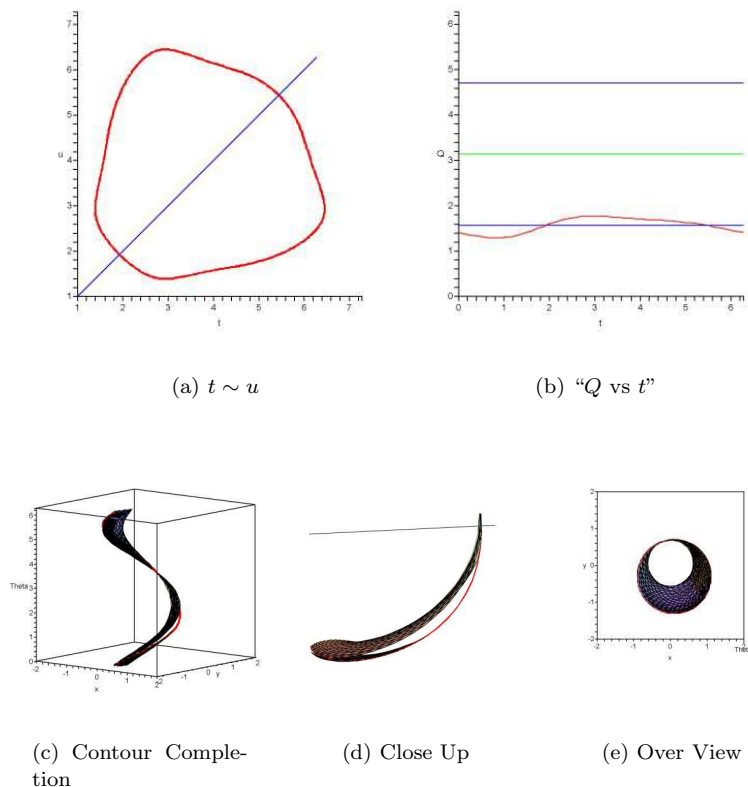
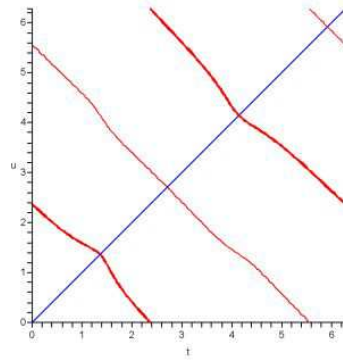
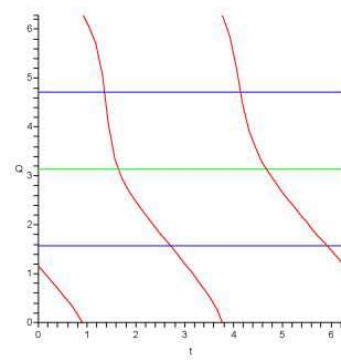
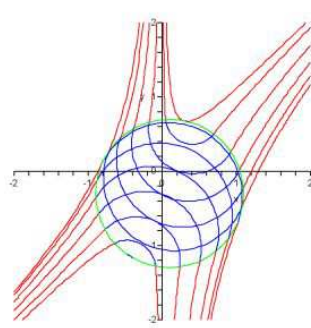


Fig. 6. $I = (1 + x^2 + 0.9y^2)^{-1}$, Centre=(0.1, -0.3), Radius=1, Connecting γ to γ .

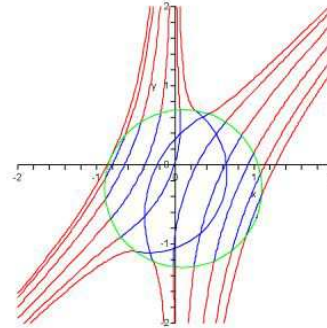
It is clear that the lift (8.2) cannot occur from an occlusion problem as it would require the vector field ∇I to be rotational and hence non-conservative. However gaps in the implicit plot are characteristic of occluded maxima and minima, at least in the absence of symmetry. See Figure 6 for an explicit example where $I = (1 + x^2 + 0.9y^2)^{-1}$ and the circle occludes a local maximum of the function. In figure 6 (a), we see that there are two gaps where there are no connections between $\gamma(t)$ and any other point on the curve. The nature of the gap as part of the minimal spanning surface is shown in the remaining graphs.

8.4. Case 4: $|\deg Q| > 1$

When Q has large degree, the phenomena of overlapping contours and immersed, discontinuous spanning surfaces occurs naturally even when we are considering only rules connecting γ to itself. In Figure 7 we return to the intensity function $I = (1 + x^2(x - y)^2)^{-1}$, but with the occluded region shifted to have centre (0.1, -0.3)

(a) $t \sim u$ (b) “ t vs Q ”

(c) Contour Completion I



(d) Contour Completion II

Fig. 7. $I = (1 + x^2(x - y)^2)^{-1}$, Centre= $(0.1, -0.3)$, Radius=1, Connecting γ to γ .

and radius 1. Since we are now occluding the saddle point (of $x(y - x)$) at $(0, 0)$, the degree of Q is -2 .

In this instance we see that Q is now a monotone two-to-one function from \mathbb{S}^1 to \mathbb{S}^1 . This corresponds to there now being two branches of the implicit plot of (8.1) in Figure 7 (a). For convenience of reference we shall refer to the highlighted branch as branch I and the other as branch II. In both contour completions there is overlap as Legendrian points are crossed while transversing the branches.

8.5. Connecting γ to $\bar{\gamma}$

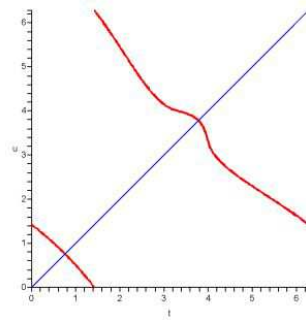
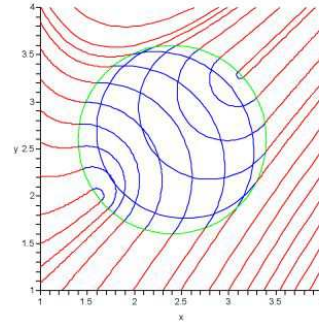
For the problem of visual completion we must consider also rules connecting the lift γ to its conjugate lift $\bar{\gamma}$. To illustrate this we return to our original example with the occluded region being the unit disc centred at $(2.4, 2.6)$. We follow the same basic program, but instead focus on the orthogonal points as our start and finish locations. Unfortunately, this introduces a pathology into the construction of our contour completion and minimal spanning surfaces. To progress from one orthogonal point to the other along a branch of the implicit plot of (7.4) it is necessary to pass through a Legendrian point. The effect of this is to switch which segment of the connecting rules projects to the interior of the occluded region. As is seen in Figure 8 (b) this causes overlaps of the contour completion. If we look at the minimal surface formed from these internal rule segments, in order to completely span γ we must continue further along the branch until we return to the original orthogonal point. This produces the discontinuous self-intersecting surface of Figure 8 (c). From the perspective of minimal spanning surfaces, it is more natural to allow rule segments that project outside the occluded region. As is shown in Figure 8 (d), this yields a smooth immersed surface between γ and $\bar{\gamma}$, but it still self-intersects.

9. A sufficient condition for effective disocclusion

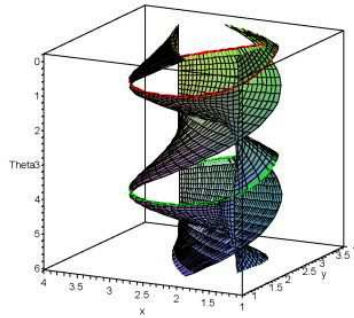
The examples of the last section point to several general features of the solutions to the occlusion problem. We will now show that under some assumptions on the image function I , we can guarantee the existence of a solution to the occlusion problem, ie. a minimal spanning surface satisfying condition III. To do so, we need some preliminary lemmata.

Lemma 9.1. *Let $I : \mathbb{R}^2 \rightarrow \mathbb{R}$ be an intensity function of an image with a completely nondegenerate occlusion given by a circular region D . Suppose there exists a minimal spanning surface Σ of the occluded region associated to a monotone function $t \rightarrow u(t)$ and so that the projection of Σ to D is not surjective. Then, one of the rules of the minimal spanning surface is a circle that, when projected to \mathbb{R}^2 lies entirely inside D and is tangent to the boundary of D at a Legendrian point.*

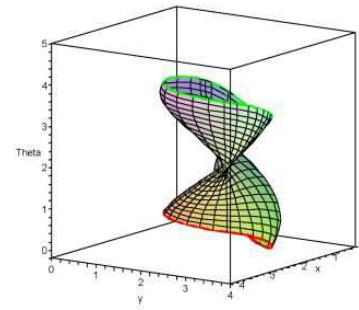
Proof: We begin with some simple geometric observations. First, if Σ is composed of circles of infinite radius (i.e. straight lines), the projection is trivially surjective. So, we may assume there are some circles in Σ that have finite radii. Second, let $\gamma(t)$ be the circle that bounds the occluded region (as above), oriented counterclockwise, and let c be a circle of finite radius connecting two points on γ that is the projection of a rule of Σ . If \vec{n} is the inward pointing normal to c , then let $s(t) = \cos(\alpha(t))$ where $\alpha(t)$ is the angle (in \mathbb{R}^2) between $\dot{\gamma}$ and \vec{n} at $\gamma(t)$. Then, if c connects $\gamma(t_1)$ to $\gamma(t_2)$, $\text{sign}(s(t_1)) = -\text{sign}(s(t_2))$ (see figure 9 (a)). Moreover, in the degenerate case where $t_1 = t_2$, the circle c is tangent to γ (i.e. $\gamma(t_i)$ is Legendrian) and thus $s(t_i) = 0$. Since u is monotone (and in particular, one to one) and R, x_c, y_c are continuous in

(a) $t \sim u$ 

(b) Contour Completion



(c) Minimal Spanning Surface I



(d) Minimal Spanning Surface II

Fig. 8. $I = (1 + x^2(x - y)^2)^{-1}$, Centre=(2.4, 2.6), Radius=1, Connecting γ to $\bar{\gamma}$.

t , s is well defined and, for $0 \leq |R| < \infty$, s is continuous. At points where $|R| = \infty$, s may have a jump discontinuity as s will switch sign at such points.

By Lemma 6.5, we have that there are at least two Legendrian points and so, by the previous discussion, the function s potentially switches sign as s is zero at a Legendrian point. Consider now a circle passing through such a Legendrian point. Then (see figure 9 (b)) if the circle is to lie outside the occluded region, then moving in the direction of the parametrization of γ , we must have that s moves from positive values to negative values. For s to change sign, we must have that the inward normal to the rule c changes direction. As we have seen, this can happen at a Legendrian point, but it may also happen if $|R|$ tends to either zero or infinity. By Lemma 7.4, R cannot be zero so we must have that either we encounter another

Legendrian point of this type or $|R| \rightarrow \infty$. Without loss of generality, we may pick the two Legendrian points so that one of the two arcs of γ that they bound contains no other Legendrian points of this type. Denote this region by $\gamma|_{(t_1, t_2)}$. Hence, we must have that $|R| \rightarrow \infty$ for some $t_0 \in (t_1, t_2)$.

To finish the proof, suppose there exists a point x in the occluded region so that the projection of Σ misses x . For each t , there exists a circle, $\bar{c}_t(s)$, connecting $\gamma(t)$ to x with $\bar{c}_t(0) = \gamma(t)$ and $\bar{c}'_t(0) = \frac{\nabla I}{|\nabla I|}^\perp(\gamma(t))$. Let $\bar{R}(t)$ be the radius of this circle and

$$\mathcal{R}(t) = \begin{cases} \bar{R}(t) & \text{if } \dot{\gamma}(t) \cdot \ddot{\bar{c}}_t(0) > 0 \\ -\bar{R}(t) & \text{if } \dot{\gamma}(t) \cdot \ddot{\bar{c}}_t(0) < 0 \end{cases}$$

So, for the projection of Σ to miss x , we must have that $\text{sign}(\cos(\alpha))R(t) \neq \mathcal{R}(t)$ for all $t \in (t_1, t_2)$. But, by the discussion above, $\text{sign}(\cos(\alpha))R(t)$ changes sign on this region and hence $\bar{R}(t)$ must also tend to ∞ and so must tend to ∞ at t_0 as well. By construction, the rule through $\gamma(t_0)$ is a straight line and hits x , contradicting the assumption that the circles at the Legendrian points lie outside D (see figure 9 (c)). ■

Lemma 9.2. *If $Q' < 0$ everywhere then the limiting rules at any Legendrian point are external to the occluded disc.*

Proof: Suppose not. Then without loss of generality we may rotate and reflect the image data to match Figure 10, where we are assuming that the curves are oriented to the counter-clockwise direction. Elementary arguments then show that the angles marked are indeed $Q(t) - \pi/2$ and $\pi/2 - Q(u)$ and that these must therefore both be positive. However at the Legendrian point we must have $Q = \pi/2$. This clearly violates the condition that $Q' < 0$. ■

Remark 9.1. We remark that if Q' is positive at a Legendrian point, then the circle tangent to the occlusion boundary may indeed lie inside the occluded circle.

Theorem 9.2. *Let $I : \mathbb{R}^2 \rightarrow \mathbb{R}$ be an intensity function of an image with an occlusion given by a circular region D . Further, suppose $\gamma \in \mathcal{RT}$ is the θ lift of ∂D and that the occlusion is completely nondegenerate and occludes no critical points of I . If $Q'(t) \neq 0$ for $t \in [0, 2\pi]$ then there exists a minimal spanning surface of γ satisfying condition II. Moreover, if $Q'(t) < 0$ for $t \in [0, 2\pi]$ then the minimal surface satisfies condition III.*

Proof: As discussed above, if the occlusion is completely nondegenerate and occludes no critical points then $\deg Q = -1$. Further, since $Q' \neq 0$, we have that the function $u(t)$, implicitly defined by

$$Q(t) + Q(u) = (2k + 1)\pi$$

is monotone. Thus, $u : S^1 \rightarrow S^1$ is one to one and onto and thus, for each t , there is a unique point connecting to t given by $u(t)$. Using the matrix equation

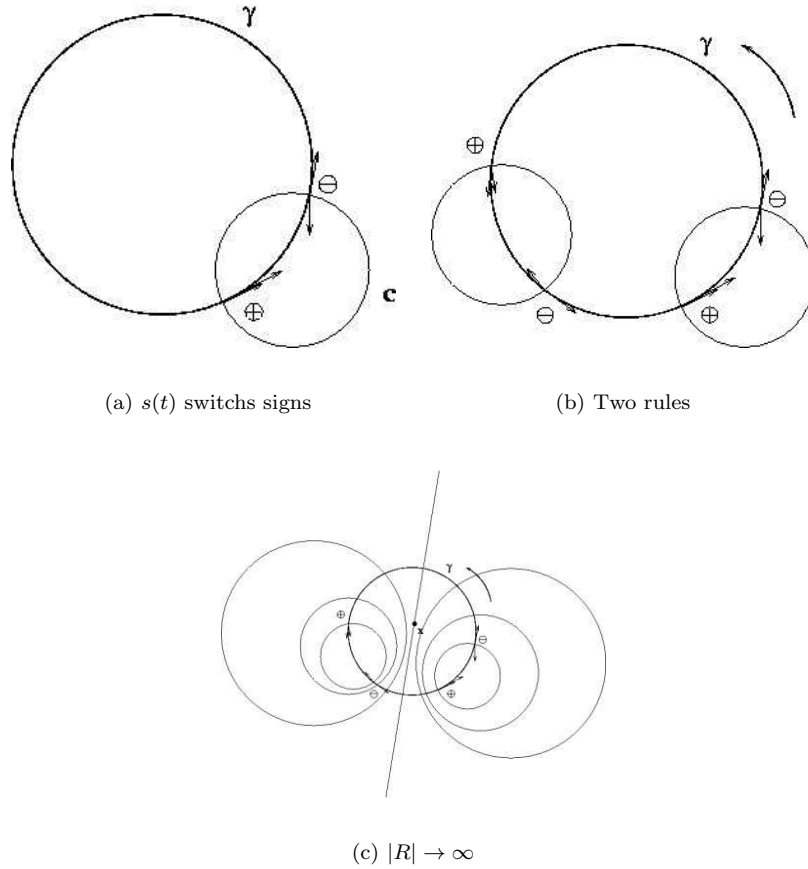


Fig. 9. Behavior of rules in a spanning surfaces

7.5 determines the rules joining t to $u(t)$ and, by picking the portion of the circle defining the rule to be inside of D when projected to \mathbb{R}^2 , we also satisfy condition II.

By Lemma 9.1 and Lemma 9.2, we have that under the assumption of $Q' < 0$, the spanning surface satisfies condition III. ■

10. Discussion

The theorem of the previous section shows that if the behavior of I near the occluded region is relatively tame, then we can easily construct a minimal surface that spans the occluded region. In figures 11 - 15, we demonstrate an implementation of the algorithm described in the previous section in cases where the theorem applies. The

32 *Robert K. Hladky and Scott D. Pauls*

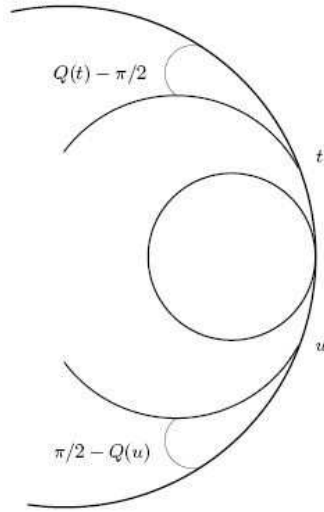


Fig. 10. Legendre Gap.

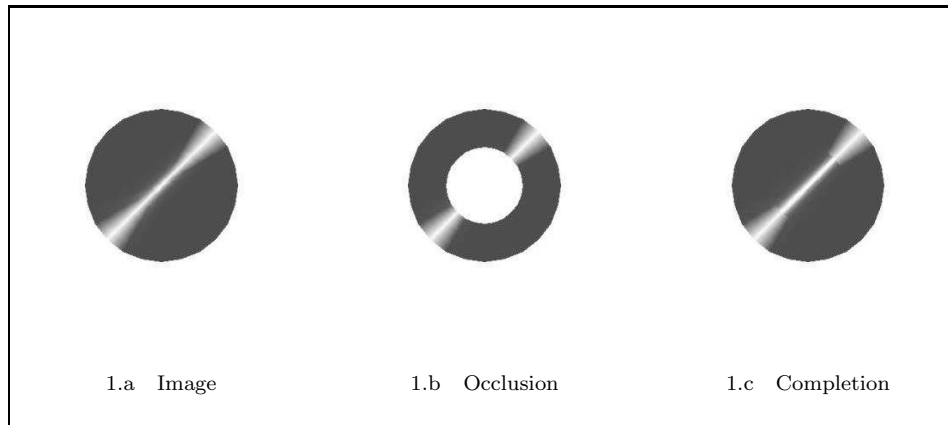


Fig. 11. Occlusion of a simple linear image

images were created by assigning color to the value of various functions (as with the previous test image).

In figure 11, we see that the algorithm easily completes a linear image using straight lines. Similarly, in figure 12, we see that when the a complicated portion of a region is occluded, it may not necessarily be recovered. In more interesting examples that show the power of this new method, figures 13 ,14, and 15 show completion using the circles identified in previous section. Figure 13 shows the completion of a curve which preserves the curvature of the original image. Figures 14 and 15 show

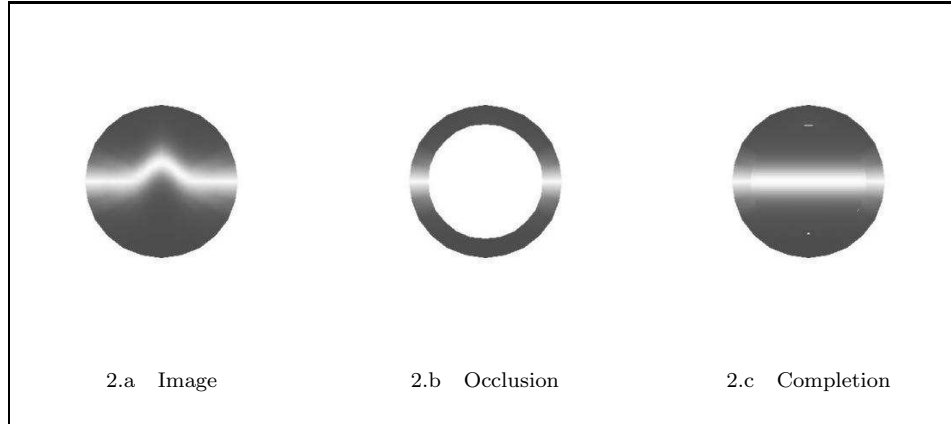


Fig. 12. Occlusion of a complicated portion of an image.

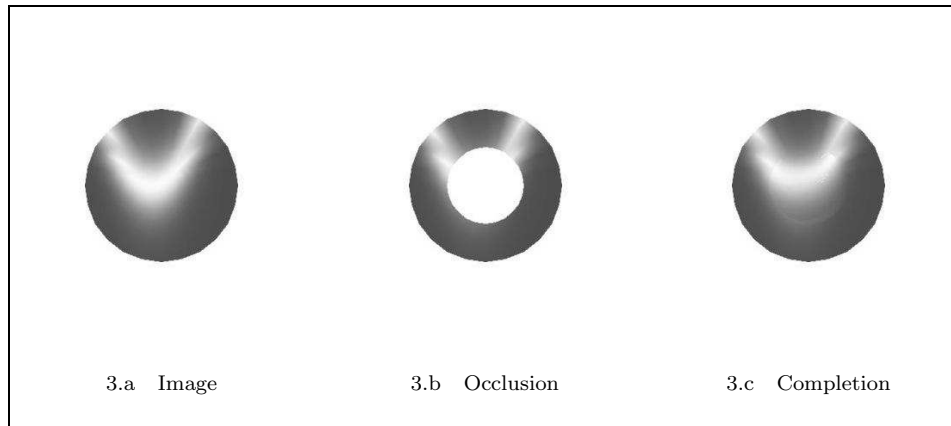


Fig. 13. Occlusion of a curve

that the algorithm preserves concavity. We note that this are features that earlier diffusion based algorithms often had trouble completing in a reliable manner.

All of the other cases presented show different types of pathology:

- (1) Case 2 shows the simplest type of failure of a spanning surface to be a graph: when Q' has zeros. In this case, we have “backtracking” of rules which causes the resulting surface derived from the implicitly defined function u to give an immersed rather than embedded surface.
- (2) Case 3 shows an instance where no smooth minimal surface exists due to the presence of non-Legendrian solitary points. As pointed out above, this behavior seems to be characteristic of occluded critical points of I . Moreover, this behavior further indicates that restricting to smooth spanning surfaces, while

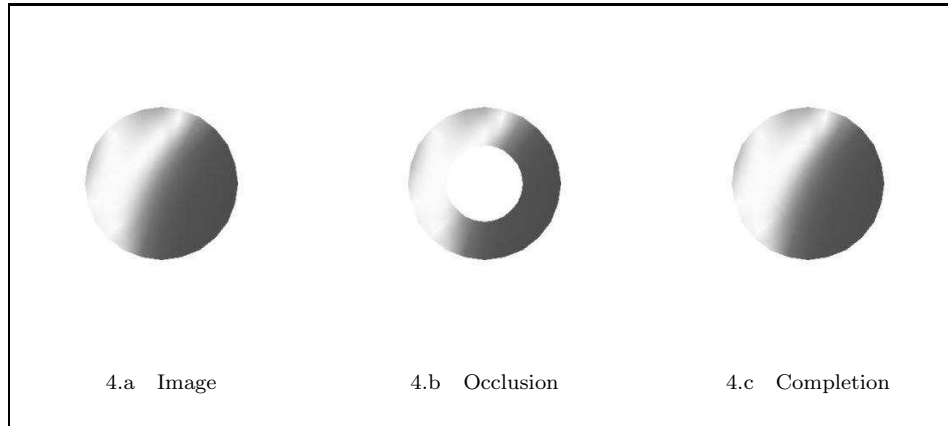


Fig. 14. Completion preserves concavity, I

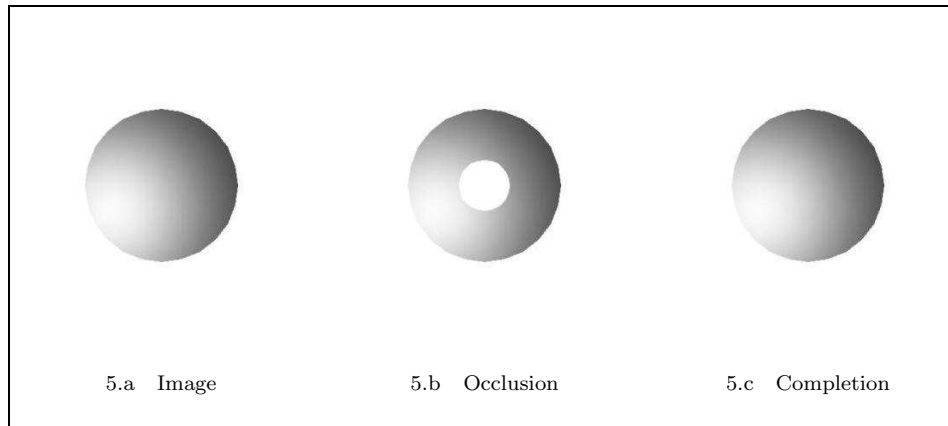


Fig. 15. Occlusion preserves concavity, II

computationally effective, will not solve any possible minimal surface problem with Dirichlet conditions. Case 2 is similar to a result to the case in the Heisenberg group²⁰ but Case 3 shows entirely new behavior stemming from the nontrivial topology of the space.

- (3) Case 4 shows that with higher degree there are potentially both nonuniqueness issues as well as problems with satisfying condition IV, i.e. forcing the spanning surface to be a graph.

The pathologies outlined above, coupled with the discussion of connection γ to $\overline{\gamma}$, lead us to several conclusions. First, the restriction to smooth spanning surfaces, while sufficient for many types of problems (such as those of theorem Theorem 9.2) is likely insufficient for more complicated areas of an image. Second, the different

types of pathologies suggest that to amodally complete a given occlusion, the “best” completion is likely to come from knitting together various pieces of several different solutions (i.e. from different branches of the curve defining u or from pieces connecting γ to $\bar{\gamma}$). Again, this points towards the necessity of a more sophisticated mechanism. However, we point out that this is consistent with the simulation data found by Citti and Sarti⁵ showing that several different possible completions are present at the same time in \mathcal{RT} after using their diffusion method. If this model of minimal surface completion is accurate reflecting the completion mechanism in V1, this ambiguity stemming from multiple (partial) solutions may be resolved by the input and feedback from other layers of the visual cortex. In particular, we note that our algorithm often produces connections between level sets of different “heights” thus creating a completion which is not ideal from the point of view of matching like intensities within the image. This is consistent with the model of the visual cortex present in section 2 as the representation of the image in \mathcal{RT} does not carry information about the intensity of the image, but only information about the level sets of the image itself. One expects that with additional input such as color/intensity information, the best possible completion could be picked out of the possibilities.

Acknowledgment

Both authors are partially supported by NSF grant DMS-0306752.

References

1. L. Ambrosio and S. Masnou. A direct variational approach to a problem arising in image reconstruction. *Interfaces and Free Boundaries*. To appear.
2. Jih-Hsin Cheng and Jenn-Fang Hwang. Properly embedded and immersed minimal surfaces in the Heisenberg group. 2004. Preprint: arxiv math.DG/0407094.
3. Jih-Hsin Cheng, Jenn-Fang Hwang, Andrea Malchiodi, and Paul Yang. Minimal surfaces in pseudohermitian geometry. 2003. Preprint.
4. G. Citti, M. Manfredini, and A. Sarti. Neuronal oscillation in the visual cortex: Gamma-convergence to the Riemannian Mumford-Shah functional. *SIAM Journal of Mathematical Analysis*, 35(6):1394 – 1419, 2003.
5. G. Citti and A. Sarti. A cortical based model of perceptual completion in the roto-translation space. 2004. Preprint.
6. Daniel Cole. *On minimal surfaces in Martinet-type spaces*. PhD thesis, Dartmouth College, 2005.
7. D. Danielli, N. Garofalo, and D.-M. Nhieu. Minimal surfaces, surfaces of constant mean curvature and isoperimetry in Carnot groups. August, 2001. Preprint.
8. Nicola Garofalo and Duy-Minh Nhieu. Isoperimetric and Sobolev inequalities for Carnot-Carathéodory spaces and the existence of minimal surfaces. *Comm. Pure Appl. Math.*, 49(10):1081–1144, 1996.
9. Nicola Garofalo and Scott D. Pauls. The Bernstein problem in the Heisenberg group. 2003. Submitted.
10. C.D. Gilbert, A. Das, M. Ito, and G. Westheimer. Spatial integration and cortical dynamics. *Proceedings of the National Academy of Sciences USA*, 93:615–622.

11. Robert Hladky and Scott D. Pauls. A disocclusion algorithm based on a model of the visual cortex. 2005. In preparation.
12. Robert K. Hladky and Scott D. Pauls. Constant mean curvature surfaces in sub-riemannian spaces. 2005. Preprint.
13. William C. Hoffman. The visual cortex is a contact bundle. *Appl. Math. Comput.*, 32(2-3):137–167, 1989. Mathematical biology.
14. D. H. Hubel and T. N. Weisel. Receptive fields, binocular interaction and functional architecture in the cat’s visual cortex. *J. Physiol.*, 160:106–154, 1962.
15. D. H. Hubel and T. N. Weisel. Functional architecture of macaque monkey visual cortex. *Proc. R. Soc. London (Biol)*, 198:1–59, 1977.
16. S. Kobayashi and K. Nomizu. *Foundations of Differential Geometry*. John Wiley & Sons, Inc., 1963.
17. G. P. Leonardi and S. Masnou. On the isoperimetric problem in the Heisenberg group \mathbb{H}^n . Preprint, 2002.
18. G. P. Leonardi and S. Rigot. Isoperimetric sets on Carnot groups. *Houston J. Math.*, 29(3):609–637 (electronic), 2003.
19. M. Nitzberg, D. Mumford, and T. Shiota. *Filtering, segmentation and depth*, volume 662 of *Lecture Notes in Computer Science*. Springer-Verlag, Berlin, 1993.
20. Scott D. Pauls. H-minimal graphs of low regularity in the Heisenberg group. *Comm. Math. Helv.* to appear.
21. Scott D. Pauls. Minimal surfaces in the Heisenberg group. *Geom. Ded.*, 104:201–231, 2004.
22. J. Petitot. The neurogeometry of pinwheels as a sub-Riemannian contact structure. *J. Physiology*, 97:265–309, 2003.
23. J. Petitot and Y. Tondut. Vers une neuro-geometrie. fibrations corticales, structures de contact et contours subjectifs modaux. *Mathematiques, Informatique et Sciences Humaine, EHESS, Paris*, 145:5–101, 1998.
24. Manuel Ritoré and César Rosales. Rotationally invariant hypersurfaces with constant mean curvature in the Heisenberg group \mathbb{H}^n . 2005. Preprint.
25. N. Tanaka. *A differential geometric study on strongly pseudoconvex manifolds*. Kinokuniya Book-Store Co., Ltd., 1975.
26. S.M. Webster. Pseudo-Hermitian structures on a real hypersurface. *J. Differential Geometry*, 13:25–41, 1978.

This figure "BackTrackCplot1.jpg" is available in "jpg" format from:

<http://arxiv.org/ps/math/0509636v1>

This figure "BackTrackLplot3d1.jpg" is available in "jpg" format from:

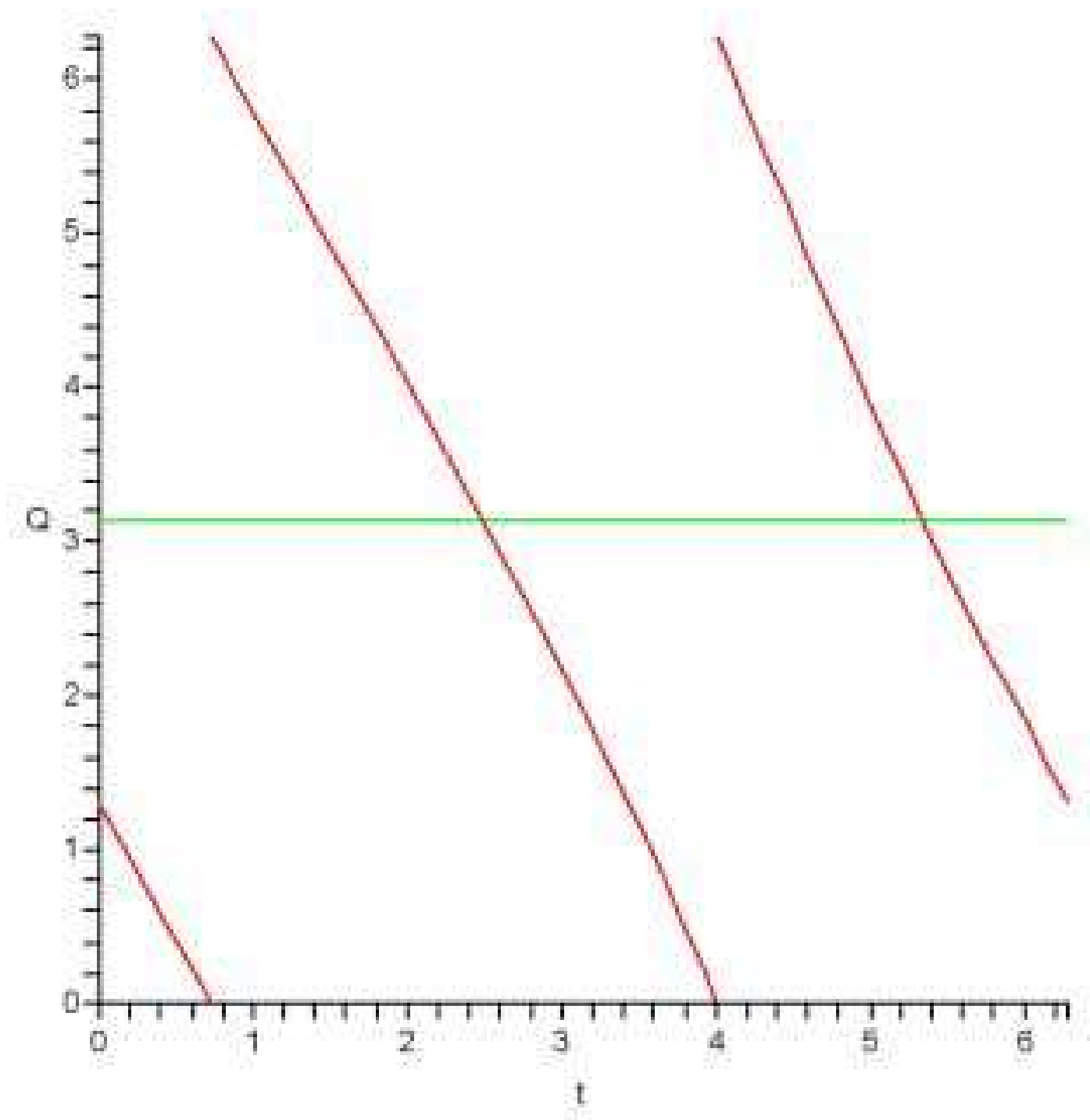
<http://arxiv.org/ps/math/0509636v1>

This figure "BackTrackQplot1.jpg" is available in "jpg" format from:

<http://arxiv.org/ps/math/0509636v1>

This figure "BackTrackUTplot1.jpg" is available in "jpg" format from:

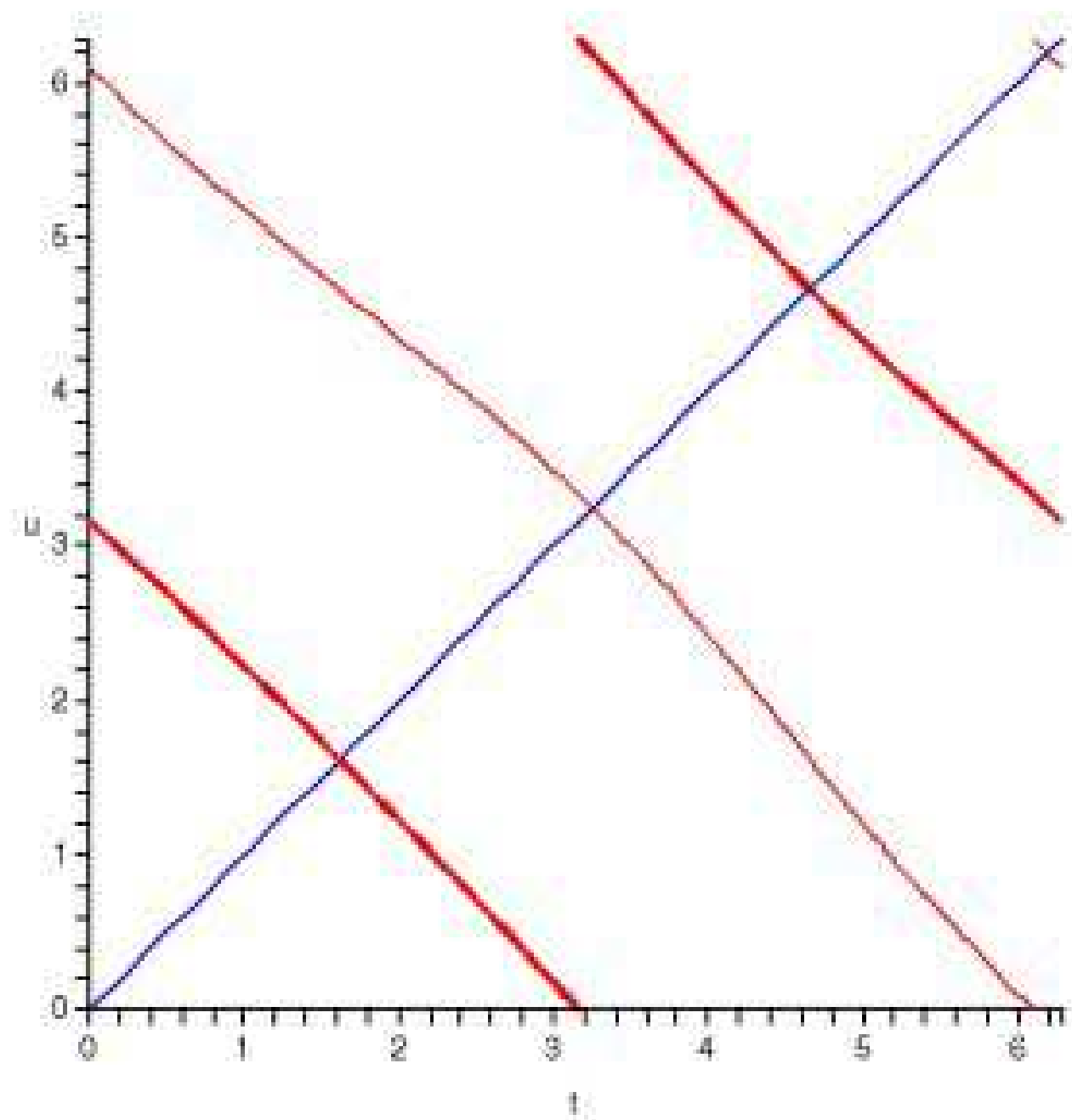
<http://arxiv.org/ps/math/0509636v1>



This figure "Basic2plot1.jpg" is available in "jpg" format from:

<http://arxiv.org/ps/math/0509636v1>

Basic Example



This figure "BasicExample.jpg" is available in "jpg" format from:

<http://arxiv.org/ps/math/0509636v1>

This figure "Basicplot1.jpg" is available in "jpg" format from:

<http://arxiv.org/ps/math/0509636v1>

This figure "Cross2plot3d1.jpg" is available in "jpg" format from:

<http://arxiv.org/ps/math/0509636v1>

This figure "DoubleC1plot1.jpg" is available in "jpg" format from:

<http://arxiv.org/ps/math/0509636v1>

This figure "DoubleC3plot1.jpg" is available in "jpg" format from:

<http://arxiv.org/ps/math/0509636v1>

This figure "DoubleQplot1.jpg" is available in "jpg" format from:

<http://arxiv.org/ps/math/0509636v1>

This figure "DoubleUTplot1.jpg" is available in "jpg" format from:

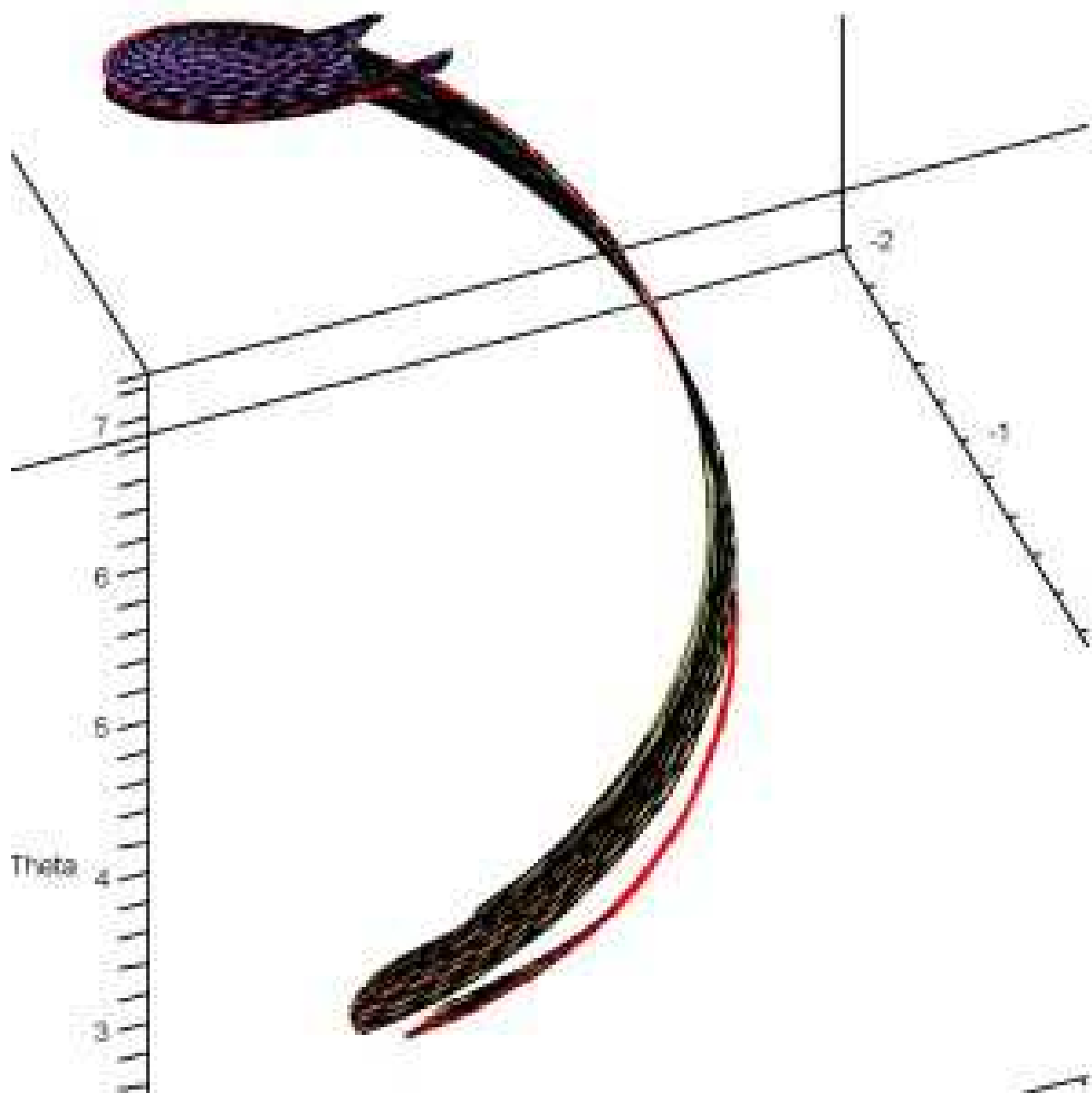
<http://arxiv.org/ps/math/0509636v1>

This figure "GapLScloseplot3d1.jpg" is available in "jpg" format from:

<http://arxiv.org/ps/math/0509636v1>

This figure "GapLSplot3d1.jpg" is available in "jpg" format from:

<http://arxiv.org/ps/math/0509636v1>



This figure "GapLcloseplot3d1.jpg" is available in "jpg" format from:

<http://arxiv.org/ps/math/0509636v1>

This figure "GapLowerplot3d1.jpg" is available in "jpg" format from:

<http://arxiv.org/ps/math/0509636v1>

This figure "GapQplot1.jpg" is available in "jpg" format from:

<http://arxiv.org/ps/math/0509636v1>

This figure "GapUTplot1.jpg" is available in "jpg" format from:

<http://arxiv.org/ps/math/0509636v1>

This figure "SimpleCCLXplot3d1.jpg" is available in "jpg" format from:

<http://arxiv.org/ps/math/0509636v1>

This figure "SimpleCCLplot3d1.jpg" is available in "jpg" format from:

<http://arxiv.org/ps/math/0509636v1>

This figure "SimpleCCplot1.jpg" is available in "jpg" format from:

<http://arxiv.org/ps/math/0509636v1>

This figure "SimpleCplot1.jpg" is available in "jpg" format from:

<http://arxiv.org/ps/math/0509636v1>

This figure "SimpleLplot3d1.jpg" is available in "jpg" format from:

<http://arxiv.org/ps/math/0509636v1>

This figure "SimpleQplot1.jpg" is available in "jpg" format from:

<http://arxiv.org/ps/math/0509636v1>

This figure "SimpleUTCplot1.jpg" is available in "jpg" format from:

<http://arxiv.org/ps/math/0509636v1>

This figure "SimpleUTplot1.jpg" is available in "jpg" format from:

<http://arxiv.org/ps/math/0509636v1>

This figure "diso_1.jpg" is available in "jpg" format from:

<http://arxiv.org/ps/math/0509636v1>

This figure "img_1.jpg" is available in "jpg" format from:

<http://arxiv.org/ps/math/0509636v1>

This figure "rtpic1.jpg" is available in "jpg" format from:

<http://arxiv.org/ps/math/0509636v1>

This figure "diso_2.jpg" is available in "jpg" format from:

<http://arxiv.org/ps/math/0509636v1>

This figure "img_2.jpg" is available in "jpg" format from:

<http://arxiv.org/ps/math/0509636v1>

This figure "diso_3.jpg" is available in "jpg" format from:

<http://arxiv.org/ps/math/0509636v1>

This figure "img_3.jpg" is available in "jpg" format from:

<http://arxiv.org/ps/math/0509636v1>

This figure "diso_4.jpg" is available in "jpg" format from:

<http://arxiv.org/ps/math/0509636v1>

This figure "img_4.jpg" is available in "jpg" format from:

<http://arxiv.org/ps/math/0509636v1>

This figure "diso_5.jpg" is available in "jpg" format from:

<http://arxiv.org/ps/math/0509636v1>

This figure "img_5.jpg" is available in "jpg" format from:

<http://arxiv.org/ps/math/0509636v1>

This figure "diso_6.jpg" is available in "jpg" format from:

<http://arxiv.org/ps/math/0509636v1>

This figure "img_6.jpg" is available in "jpg" format from:

<http://arxiv.org/ps/math/0509636v1>

This figure "legendre.jpg" is available in "jpg" format from:

<http://arxiv.org/ps/math/0509636v1>

This figure "occl_1.jpg" is available in "jpg" format from:

<http://arxiv.org/ps/math/0509636v1>

This figure "occl_2.jpg" is available in "jpg" format from:

<http://arxiv.org/ps/math/0509636v1>

This figure "occl_3.jpg" is available in "jpg" format from:

<http://arxiv.org/ps/math/0509636v1>

This figure "occl_4.jpg" is available in "jpg" format from:

<http://arxiv.org/ps/math/0509636v1>

This figure "occl_5.jpg" is available in "jpg" format from:

<http://arxiv.org/ps/math/0509636v1>

This figure "occl_6.jpg" is available in "jpg" format from:

<http://arxiv.org/ps/math/0509636v1>

This figure "rthyper.jpg" is available in "jpg" format from:

<http://arxiv.org/ps/math/0509636v1>

This figure "switchsign.jpg" is available in "jpg" format from:

<http://arxiv.org/ps/math/0509636v1>

This figure "switchsigna.jpg" is available in "jpg" format from:

<http://arxiv.org/ps/math/0509636v1>

This figure "switchsignb.jpg" is available in "jpg" format from:

<http://arxiv.org/ps/math/0509636v1>